A Study of Seizure Prediction Based on EEG Phase Synchronization

Vadim Smolyakov

Thesis submitted to University of Toronto in partial fulfillment
of the requirements for the degree of Bachelor of Applied Science

Division of Engineering Science
Faculty of Applied Science and Engineering

University of Toronto
April 14, 2009

Abstract

Around 0.6-0.8% of the world's population is affected by a re-current neurological disorder of epilepsy. Second only to stroke, epileptic seizures interrupt lives of 50 million people. The sudden and seemingly unpredictable nature of seizures is one of the most defeating facts of epilepsy. The ability to predict a rising seizure reliably can mitigate the severity of the disorder and open up new theraupetic possibilities: closed-loop seizure prevention systems and EEG triggered on-demand therapy. No study has yet reported a method that can reliably predict a seizure. This thesis investigates EEG phase synchronization as a promising algorithm for seizure prediction. The algorithm is evaluated on a database of three patients with a total of 30 seizures and 230 hours of labeled EEG data. The results of the study show 37% sensitivity for an average seizure occurrence period (SOP) of 30 minutes and maximum false prediction rate (FPR_{max}) of 0.15 seizures/hr. A review of seizure prediction research and methodology is presented. Motivated by potential implementation on an implantable chip, a realizable FPGA architecture of the algorithm is proposed.

Acknowledgements

I would like to thank my advisor Professor Roman Genov for pointing me to the prominent researchers in the field of seizure prediction, for his encouragement and enthusiasm communicated in meetings and stimulating discussions.

I appreciate the kindness of Professor Paul Chow in providing a Xilinx board for the FPGA component of this thesis.

I would like to thank a group of researchers in University of Freiburg, Germany, for providing the EEG dataset used in this work and establishing an international workshop to advance the study of seizure prediction.

Finally, I thank my parents for their ever-present guidance and support.

Contents

List of Figures

List of Tables

Part I

Introduction

Chapter 1

Introduction to Seizure Prediction

1.1 Overview: Seizure Prediction

1.1.1 Introduction

The research in seizure prediction is focused on developing methods for *reliable prognosis* of seizures suitable in clinical application. The prediction is commonly based on time-window analysis of patients' electroencephalogram (EEG) recording. For each window of EEG, a certain characterizing measure is computed and used to warn the patient of an impending seizure.

Seizure prediction is a growing research field. To date, no study has provided a single algorithm capable of predicting a seizure with high sensitivity and low enough false prediction rate. The field of seizure prediction has in many ways been influenced by parallel advances in physics and mathematics [14]. For example, an EEG signal may be regarded as a varying non-linear time series. Thus, non-linear techniques previously used in physics have been recently applied to the field of seizure prediction.

A promising non-linear prediction algorithm is identified and evaluated in this study based on EEG recordings of *three* patients for a total of *230* hours of EEG, *10* seizures per patient. Recent work in seizure prediction resulted in the development of rigorous methodology to assess predictive performance of different characterizing measures. A set of guidelines and future research requirements have been proposed in [5]. Such methodology was examined and adopted in the present

study. Moreover, the potential for on-chip implementation of the selected algorithm is explored by proposing FPGA implementation of the algorithm.

The *motivation* for seizure prediction, and the *scope and purpose* of this study is presented in the following Sections 1.1.2 and 1.1.3. Section 1.1.4 details the *organization* of the thesis.

1.1.2 Motivation

Epilepsy is one of the most common neurological disorders, second only to stroke, with a prevalence of 0.6-0.8% of the world's population [13]. Epilepsy affects people of all ages. Around 50 million people worldwide suffer from re-current and sudden neurological disease of seizure [23].

In the majority of cases, seizures occur unexpectedly, without a sign of warning to alert and prepare the person for an onset of seizure. Such abrupt and uncontrollable nature of the disease can cause physical injury. In addition to bodily harm, there is a feeling of helplessness associated with a lack of control over seizure and inability to anticipate and know when a seizure may strike.

A system that can reliably predict a prospective seizure can have a significant impact on the patient's life. A reliable prediction algorithm can alleviate patient's anxiety and open up new therapeutic possibilities: closed-loop seizure-prevention systems [10], EEG-triggered on-demand therapy [2] and electrical stimulation [20].

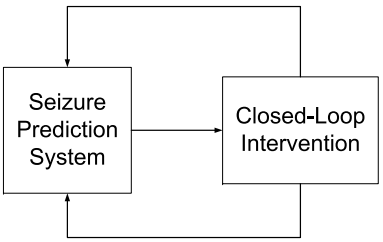

Figure 1.1: Seizure Prediction Closed-Loop System

In order to adopt a seizure prediction algorithm in clinical practice, it must pass rigorous statistical validation using real EEG data. To date, no study has reported an algorithm reliable enough for

clinical application. Yet, evidence has accumulated that certain measures, particularly measures that quantify interaction between different brain regions, show a promising performance as evidenced by statistical validation [5]. The study, characterization and implementation of such an algorithm is the subject of this thesis.

1.1.3 Purpose

The study of seizure prediction is aimed, on a higher level, at improving the condition of people suffering from epilepsy by means of a reliable prediction technique able to anticipate the seizure and apply a corrective action. A technique that can be realized on an implantable chip and meet the standards of clinical application.

Towards this goal, the *purpose* and *scope* of the thesis is to achieve the following:

1. To understand the state and methodology of the field of seizure prediction
2. To select and describe a promising algorithm suitable for on-chip implementation
3. To analyze, tune and evaluate the algorithm on a real EEG dataset via Matlab implementation
4. To propose a hardware implementation of the algorithm on FPGA
5. To evaluate results, draw conclusions, and offer future perspective

1.1.4 Organization

The thesis is structured in *four* parts.

Part I presents the *literature review* of the field of seizure prediction: the background, current state of the field and future milestones are introduced in Section 1.2. Section 1.3 identifies prominent seizure prediction algorithms and provides a description of *two* remarkable algorithms.

Part II focuses on EEG Phase Synchronization *algorithm* and *its evaluation*. Section 2.2 presents reasons for selection and provides detailed description of the algorithm. Section 2.3 outlines experimental variables, patient data, procedure, and evaluation of the prediction technique. Experimental results are analyzed and discussed in Section 2.4. Future work is proposed at the end of the section. Part II concludes with a summary of predictive performance of EEG Phase Synchronization algorithm.

Part III describes the *implementation* of EEG Phase Synchronization algorithm. Section 3.1 details Matlab implementation: functional overview of main signal processing blocks and their verification. Section 3.2 proposes FPGA implementation of the algorithm. Technology selection and architectural overview is presented in this section.

Part IV concludes the thesis with a summary of results and a discussion on future work.

1.2 Background: Understanding the Field

1.2.1 Formative Years

The field of *seizure prediction* has been influenced by advancements in physics, mathematics and economics related to prediction of uncertain and rare events. Dating back to 1975, the field was largely shaped by the analysis techniques available at the time.

In the 1970s and 1980s researchers considered mainly linear techniques such as spectral data and pattern recognition along with mathematical modeling of EEG signals [14]. Early findings showed that pre-ictal states could be detected based on EEG pattern seconds before the onset of seizure.

Beginning in the 1990s, the linear methods were used in addition to methods of non-linear dynamics, involving measures such as Lyapunov exponents, entropy, and correlation densities. A number of studies in the 1990s showed characteristic pre-ictal changes minutes to hours before seizure onset and were interpreted as interictal states of various duration.

Almost all of the mentioned approaches used univariate measures related to a single recording electrode and little attention was given to the relationship between different recording sites. If one views a seizure as a simultaneous action of a network of neurons, additional insight can be gained by studying combination of electrodes from different recording sites. Thus, in the past decade researchers focused on bivariate and multivariate measures. These techniques include phase synchronization, cross-correlation, and difference of largest Lyapunov exponents among others [14].

Much of the EEG data used at that time was restricted to only the ictal period and it was highly selected based on the seizure type, signal to noise ratio, duration of the recording, and presence of artifacts. The lack of clear definitions and unified methodology prompted the creation of International Seizure Prediction Group (ISPG) in 2000 to improve the structure of research in the field of seizure prediction.

In 2003, a number of studies were published that found a substantially poorer predictive performance than previously reported optimistic results. Earlier highly-optimized algorithms applied to small, selected data sets could not be reproduced on unbiased EEG recordings [5].

The first attempts for testing seizure prediction algorithms in a prospective way were carried out by Iasemidis (2003) [17] and D'Allesandro (2005) [18].

1.2.2 State of the Field

At present, it is not clear which of the characterization measures are best suited for prospective prediction of seizures. There are indications [19], [7], [8] of superior performance for measures characterizing *relations* between brain regions, consistent with the view of a seizure as a synchronous action of a *network of neurons*.

Some studies [18], [15] demonstrated that a combination of measures is likely required to carry out reliable seizure prediction for individual patients.

1.2.3 Future Milestones

For the field of seizure prediction to meet the benchmark of clinical application, it is necessary to use unified methodology and rigorous statistical validation. The following guidelines are proposed in [5]:

- Prediction algorithms should be tested on unselected continuous long-term recordings covering several days of EEG
- Studies should assess both sensitivity and specificity and should report these quantities with respect to the applied prediction horizon. Rather than false prediction rates, the portion of time under false warning should be reported
- Results should be tested using statistical validation methods based on Monte Carlo simulations or naive prediction schemes to prove that a given prediction algorithm performs indeed above chance level
- If prediction algorithms are optimized using training data, they should be tested on independent testing data. Performance of an algorithm should always be reported separately for the testing data.

The items above provide next milestones in the field of seizure prediction.

1.3 Seizure Prediction: Algorithms

1.3.1 Overview

All prospective prediction algorithms rely on window analysis techniques. Each window of Electroencephalogram (EEG) data is processed and a characterization measure describing the seizure state is computed. This measure provides the input to a prediction device which triggers an alarm in case of an impending seizure. The prediction decision is a function of the patient's nominal (inter-ictal) and current characterization measures.

1.3.2 Classification

A seizure prediction algorithm can be classified into *three* main categories based on *causality*, *linearity* and the *number of inputs* used to compute a prediction.

Algorithmic and Statistical

Statistical analysis is non-causal, retro-spective analysis of EEG. In statistical analysis, EEG is divided into assumed blocks of pre-ictal, inter-ictal, and ictal data used for processing and training of the parameters. The temporal sequence of EEG segments need not be preserved in statistical analysis. The main advantage of statistical analysis is in performance comparison of different characterization indices.

Algorithmic approach computes a characterizing measure for each time profile window. This class of algorithms represents causal analysis suitable for on-chip implementation.

Linear and Non-linear

Linear and non-linear characterizing measures have been used to study EEG dynamics. Linear techniques provide simple means of analyzing statistical and spectral information of the EEG signal, whereas non-linear measures take advantage of the non-linearities present in EEG.

Common *linear* techniques include *statistical moments*, *spectral band power*, and *autocorrelation function*. To illustrate a linear prediction algorithm, consider the autocorrelation function for time series:

$$A(\tau) = \frac{1}{(N-1)\sigma^2} \sum_{i=1}^{N-\tau} x_i x_{i-\tau} \tag{1.1}$$

where $\tau = 0, .., N-1$ and σ^2 represents the variance. By construction, $A(\tau)$ varies between -1 and 1, reaching 1 at time delay of zero: $A(0) = 1$. For non-periodic time series, the autocorrelation function decays from $A(0)$ as the values of τ increase. The slower $A(\tau)$ decays from the origin, the stronger is the correlation between the input channels. Thus, an estimate of the strength of linear correlation can be defined using the first zero crossing:

$$\tau_0 = \min(\tau | A(\tau) = 0) \tag{1.2}$$

Therefore, linear correlation provides a means of characterizing a pair of EEG signals.

Non-linear time series properties of the EEG signal are utilized by non-linear techniques. Common non-linear methods include the *correclation sum*, *largest Lyapunov exponent*, and *phase synchronization*.

To appreciate non-linear prediction measures, consider an example of largest Lyapunov exponent L_{max}. L_{max} is used to compute exponential divergence of nearby trajectories in a state space. L_{max} can be computed from time series directly [1]. However, the computation suffers from the presence of noise and is highly dependent on the state space parameters, in addition to being computationally expensive. In order to overcome these obstacles, an estimate of L_{max} can be computed as follows:

$$d_j(i) \approx C_j e^{L_{max} i \Delta t} \tag{1.3}$$

where $d_j(i)$ is the average divergence between two trajectory segments at time t_i and C_j with $j = 1, .., M$ a constant given by initial separation of a reference vector $\overline{z_j}$ in state space and its nearest neighbor.

Taking natural logarithm of the expression above:

$$\ln d_j(i) \approx \ln C_j + L_{max} i \Delta t \tag{1.4}$$

Re-arranging and averaging over j:

$$L_{max} = \frac{1}{\Delta t} \langle \ln d_j(i) - \ln C_j \rangle \tag{1.5}$$

The calculated largest Lyapunov exponent L_{max} provides a non-linear measure of the divergence of a pair of EEG signals.

It is important to note that the presence of non-linearity in EEG does not in itself justify the use of non-linear, complicated measures to characterize dynamic changes in the EEG, rather both measures must be verified and tested on their prediction ability to justify their use [5].

For a complete list of characterization measures used in seizure prediction, see Table 1 of [5]. A brief mathematical description of each measure can found in Appendix A of [7].

Univariate and Multivariate

All seizure prediction algorithms can be further classified based on the number of inputs used to compute the prediction into *univariate*, *bivariate*, and *multivariate* methods.

Univariate prediction algorithms, such as autocorrelation and spectrum analysis methods, use data from a single EEG channel. Whereas bivariate, or more generally, multivariate methods use two or more EEG electrodes to compute a single characterizing measure.

Note that the use of univariate prediction method does not limit the analysis to a single electrode, rather a number of EEG electrodes are processed in parallel: a univariate measure is computed for each electrode and the results form the input to the prediction device.

1.4 Conclusions

The field of seizure prediction offers favorable ground for research. The methodology and future directions of the field have been outlined in the literature [5]. Long-term, continuous EEG recordings are available through the International Seizure Prediction Project [24] and an extensive list of algorithms is published in Table 1 of [5]. Yet, no single algorithm was found to yield sensitivity of clinical importance. This creates an opportunity for research in seizure prediction with a potential direction towards an implantable chip implementation.

The following Table 1.1 captures some of the main types of causal measures suitable for on-chip implementation:

Algorithmic	**Linear**	**Non-Linear**
Univariate	Statistical Moments Spectral Band Power Autocorrelation Function	Correlation Sum Largest Lyapunov Exponent Algorithmic Complexity
Bivariate	Linear Cross-Correlation Linear Coherence	Non-Linear Interdependence Phase Synchronization Dynamical Entrainment

Table 1.1: Algorithm Types

Chapter 2

The Method of Phase Synchronization

2.1 Introduction

Seizure prediction based on EEG Phase Synchronization algorithm is the subject of Part II. It is organized in *three* sections. *First*, the reasons for selecting the algorithm are presented along with detailed description in Section 2.2. *Secondly*, the experimental methodology used to evaluate the algorithm is fully described in Section 2.3. *Thirdly*, experimental results are discussed and evaluated in Section 2.4. Part II concludes with evaluation of predictive performance of Phase Synchronization algorithm.

2.2 EEG Phase Synchronization

2.2.1 Reason for Selection

There are *two* reasons for selecting EEG Phase Synchronization (EPS) as the seizure prediction algorithm: superior performance under statistical validation and potential for on-chip implementation.

Superior Performance

There is evidence that characterization measures relating different recording sites appear to perform significantly better than a random predictor even under rigorous statistical validation [14].

Given the bivariate nature of phase synchronization, it is possible to analyze the correlation of phase of a pair of EEG signals across different recording sites.

Epileptic seizures can be viewed as excessive and hyper synchronous activity of neurons in cerebral cortex. Thus, intuitively, a change in synchronization can be used in defining the boundaries between non-seizure and seizure states. Therefore, a prediction method that characterizes *synchronization* among different sites, can itself be considered *a priori* advantage.

On-Chip Implementation

EEG Phase Synchronization (EPS) is a causal algorithm with high potential for on-chip implementation.

Phase synchronization is widely used in the field of digital communications. Thus, main algorithmic blocks have already been proven in application and hardware. An example of such block is the Hilbert Transform [22]. The transform can be approximated by an FIR filter; thus, significantly reducing computational requirements [Appendix A].

In addition, previous studies [12] attempted to implement signal processing of non-linear time series on FPGA. Whereas the application of [12] was sensory data processing for structural health monitoring, similar implementation procedure can be applied to EEG algorithm for seizure prediction.

Therefore, phase synchronization provides a promising prediction method with a potential for on-chip implementation.

2.2.2 Detailed Description

EEG phase synchronization fits in the class of algorithmic, non-linear, bivariate characterization measures.[1] This method provides a causal analysis of non-linear time series characteristic of EEG based on two EEG inputs. The algorithm computes a characterizing measure proportional to the amount of synchronization between the pair of EEG electrodes.

Phase synchronization is defined in term of phase lock between the two signals [4]:

$$\phi_x(t) - \phi_y(t) = const \tag{2.1}$$

For each time window of EEG, a characterization index γ is computed for the two input channels as follows:

$$\gamma = \frac{1}{N}\left|\sum_{k=0}^{N-1} e^{j[\phi_x(kT)-\phi_y(kT)]}\right| = 1 - V_c \tag{2.2}$$

where γ is the measure of phase synchronization, N is the length of the discrete time sequence, T is the sampling rate, $|.|$ denotes absolute value and V_c is circular variance [16].

When the phases of sampled continuous time signals are equal, phase synchronization index γ is unity. In the opposite case of unsynchronized signals, γ is zero. This defines a decision range on γ for seizure prediction: $\gamma \in [0, 1]$.

In order to compute phase synchronization, it is first necessary to obtain the phase of the input signal. In the case of a complex scalar $z = a + jb$, the phase is given by:

$$\phi_z = \arctan(\frac{b}{a}) \tag{2.3}$$

Extending the definition above to real time series[2]:

[1] See Section 1.3.2 for algorithm classification
[2] See Appendix A.2 for justification

$$\phi(t) = \arctan(\frac{\tilde{s(t)}}{s(t)}) \tag{2.4}$$

where $\tilde{s(t)}$ is the Hilbert Transform of $s(t)$ [22]. The *ideal* Hilbert Transform shifts the phase of its input signal by $\pi/2$. However, an *FIR approximation* to the ideal transform used in this study, adds linear phase of the FIR filter to the input. Therefore, each constituent single-tone frequency of the input signal is delayed by an amount proportional to the linear phase delay at that frequency. [Appendix A.2] In the case of a complete match between two EEG time profiles, the difference in $\phi(t)$ for each channel will be zero over the observation window.

The computation of index γ defines the challenges to be overcome in hardware implementation of this algorithm. Expanding the equation for γ and substituting the phase difference $\phi_{xy}(kT)$ for $\phi_x(kT) - \phi_y(kT)$, we obtain:

$$\begin{aligned}
\gamma &= \frac{1}{N}\left|\sum_{k=0}^{N-1} e^{j[\phi_{xy}(kT)]}\right| \\
&= \frac{1}{N}\left|\sum_{k=0}^{N-1} \cos\phi_{xy}(kT) + j \times \sum_{k=0}^{N-1} \sin\phi_{xy}(kT)\right| \\
&= \frac{1}{N}\sqrt{(\sum_{k=0}^{N-1} \cos\phi_{xy}(kT))^2 + (\sum_{k=0}^{N-1} \sin\phi_{xy}(kT))^2}
\end{aligned} \tag{2.5}$$

Considering the equation above, to realize characterization measure γ, the following functions must be implemented: $\arctan(x)$, $\sqrt{x}$, $\sin(x)$, $\cos(x)$, in addition to $\tilde{s(t)}$, the Hilbert Transformer [22]. Functional implementation is detailed in Chapter 3.

2.3 Methodology

2.3.1 Patient Data

The predictive ability of EEG Phase synchronization can only be verified on a comprehensive EEG database which includes continuous, long-term EEG recording of several patients covering inter-ictal as well as ictal periods. Such dataset was found [24] and used in this thesis.

Experimental data selected for algorithm evaluation contains EEG time profiles of *three* patients, recorded and labeled during an invasive pre-surgical epilepsy monitoring at the Epilepsy Center of the University Hospital of Freiburg, Germany. The data is made available through International Seizure Prediction Project [24] with the purpose of developing a seizure prediction algorithm capable of meeting the standards for clinical application. This dataset is consistent with the guidelines proposed by the International Seizure Prediction Group (ISPG).[3]

Data Acquisition

The patient EEG data was acquired using a Neurofile NT digital video EEG system with 128 channels, 512 Hz sampling rate, and a 16 bit analog-to-digital converter. Intractranial grid, strip, and depth electrodes were used to acquire the data. EEG was analyzed and labeled by certified epileptologists [24].

Electrode Selection

Given N recording sites, there are N *choose* 2 ways of forming a pair. For computational reasons, it is necessary to limit the number of pairs while keeping important experimental data. Thus, electrode selection was done to constrain the sample space of recording electrode-pairs while preserving important experimental differences.

The following variables were identified and used for electrode pair selection for each patient [Table 2.1]

[3] See Section 1.2.3 for guidelines on research in seizure prediction

Criteria	Options
Electrode Type	Depth, Strip, Grid
Proximity to Epileptic Focus	Adjacent Sites, More than 3 sites apart
Proximity of Recording Sites	Adjacent Sites, More than 3 sites apart
Sharing of Electodes	Not shared, Shared in at least one paring

Table 2.1: EEG Electrode Selection Variables

Effort was made to include every combination of the variables above in selecting electrodes for each patient. Preference was given to adjacent recording sites, shared on the same electrode, closest to the epileptic center.

Patient 1

Patient 1 data is summarized in Table 2.2

Electrode implantation scheme is presented in Figure 2.1

Patient	Data
Age:	30
Hours of EEG:	98
No. of Seizures:	10
No. of Channels:	60
Sampling Rate:	512 Hz
Electrode Types:	Depth, strip
Sex:	Female
Diagnosis:	Focal cortical dysplasia
Epilepsy Surgery:	left temporolateral resection sparing the hippocampus
Surgery Outcome:	Engel Ia
Seizures Recorded:	Simple-Partial, Complex-Partial, Secondarily generalized tonic-clonic

Table 2.2: EEG Data: Patient 1

Patient 2

Patient 2 data is summarized in Table 2.3

Electrode implantation scheme is presented in Figure 2.2

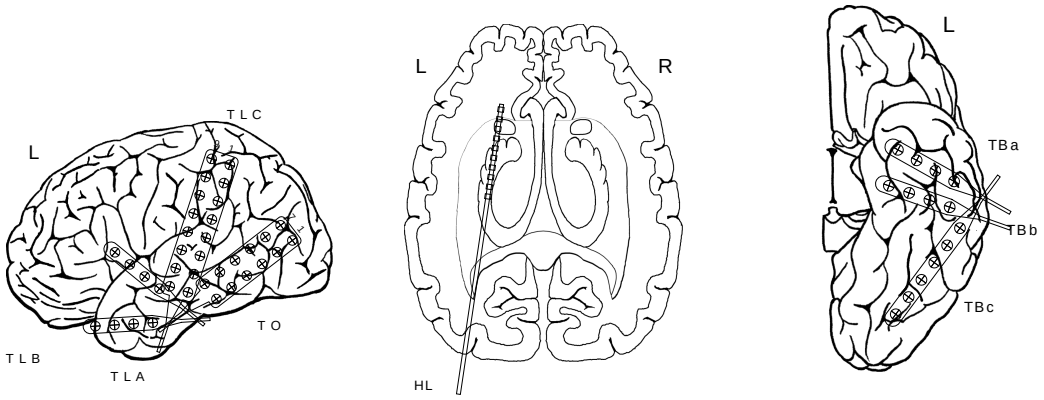

Figure 2.1: Implantation Scheme: Patient 1

Patient	**Data**
Age:	17
Hours of EEG:	30
No. of Seizures:	10
No. of Channels:	44
Sampling Rate:	512 Hz
Electrode Types:	Grip, strip
Sex:	Male
Diagnosis:	Left temporal tumor
Epilepsy Surgery:	Resection of tumor
Surgery Outcome:	Engel Ia
Seizures Recorded:	Simple-Partial, Complex-Partial, Secondarily generalized tonic-clonic

Table 2.3: EEG Data: Patient 2

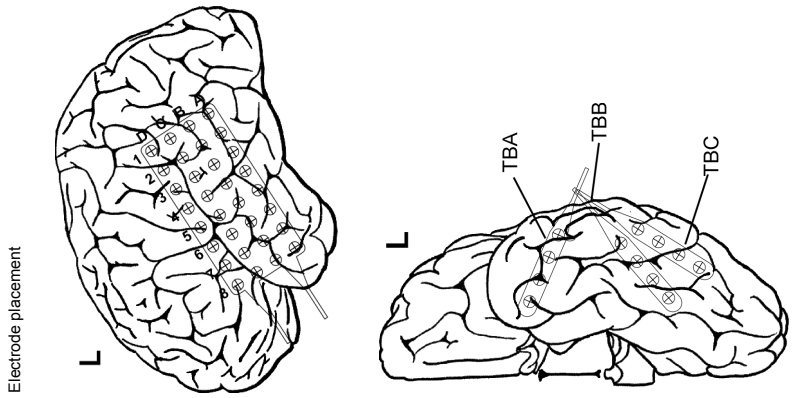

Figure 2.2: Implantation Scheme: Patient 2

Patient 3

Patient 3 data is summarized in Table 2.4

Electrode implantation scheme is presented in Figure 2.3

Patient	**Data**
Age:	10
Hours of EEG:	102
No. of Seizures:	10
No. of Channels:	22
Sampling Rate:	512 Hz
Electrode Types:	Depth, strip
Sex:	Male
Diagnosis:	hippocampal sclerosis, mesiotemporal focal cortical dysplasia and additional right occipital lesion of unknown histology
Epilepsy Surgery:	Selective right amygdalo-hippocampectomy
Surgery Outcome:	Engel Ia
Seizures Recorded:	Simple-Partial, Complex-Partial, Secondarily generalized tonic-clonic

Table 2.4: EEG Data: Patient 3

2.3.2 Experimental Variables

This section introduces the *three* metrics responsible for predictive performance of the algorithm: Maximum Seizure Occurrence Period (SOP_{max}), Minimum Seizure Prediction Horizon (SPH_{min}), and Maximum False Prediction Rate (FPR_{max}). All three metrics must be considered together in evaluating the sensitivity of the algorithm.

SOPmax: Maximum Seizure Occurrence Period

An *ideal* seizure predictor will point to the *exact* location in time at which a seizure will occur. To allow for uncertainty in the prediction, Seizure Occurrence Period (SOP) is introduced. SOP is defined as the *period of time* during which a seizure is expected to occur. Thus, SOP accounts for non-ideality of the seizure predictor.

The chosen intervention system defines the *maximum* seizure occurrence period SOP_{max}. Since a seizure may not occur at the beginning of SOP, an intervention system, such as electrical stimu-

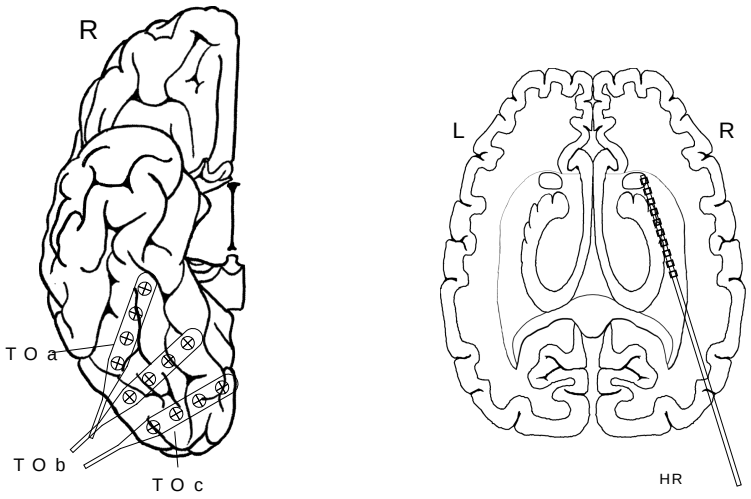

Figure 2.3: Implantation Scheme: Patient 3

lation or anti convulsive drug delivery, may require to have its effect last for the complete seizure occurrence period. Thus, the risk of side effects due to prolonged intervention sets an upper bound on SOP. In addition, higher values of SOP_{max} cause further stress and anxiety for the patient, as the predicted seizure is expected to occur at any point during the SOP. A common, acceptable range for SOP varies from 5 to 50 minutes depending on the patient and the intervention system.

SPHmin: Minimum Seizure Prediction Horizon

In order to suppress a seizure, a certain period of time is required for a corrective action between the initial prediction and the expected seizure occurrence period (SOP). This window of time is defined as the Seizure Prediction Horizon (SPH). SPH measures how far ahead in the future a given prediction algorithm can anticipate a prospective seizure.

The choice of intervention system limits the SPH. For example, an implantable system [10] that uses electrical stimulation may suppress a seizure in seconds, allowing for a very short SPH. On the other hand, a system that employs epileptic drug delivery may need an SPH of 20 to 30 minutes to suppress the seizure [21]. Therefore, the time required by intervention system determines

the *minimum* seizure prediction horizon.

In addition, longer SPH allows one to prepare for an arising seizure. The person will have more time to escape harmful surroundings such as a crowded street or a public transit.

FPRmax: Maximum False Prediction Rate

An ideal, error-free prediction is unlikely realistic and errors are bound to occur. Since false predictions cannot be completely eliminated, they must be constrained through the measure of Maximum False Prediction Rate (FPR_{max}).

False prediction rate (FPR) is defined as the number of false predictions in a given interval of time [Appendix B]. Similarly, FPR_{max} is the *maximum acceptable* false prediction rate. FPR_{max} depends on the selected intervention system. For example, for a simple warning system, high FPR will either cause the patient to not take the prediction seriously or suffer psychological distress from counting every prediction as true. The situation gets worse in the case of a drug-release intervention: the side effects due to a high intervention rate caused by false alarms can only add to the disease. Therefore, a Maximum False Prediction Rate FPR_{max} must be defined based on the intervention system and the patient.

A seizure prediction algorithm must satisfy a certain FPR_{max} to be eligible for clinical application. An average number of seizures per hour can be used as in indicator for FPR_{max}. Under normal conditions, patients with pharmacorefractory focal epilepsy have a mean seizure frequency of about three seizures per month [11] or 0.0042 seizures per hour. However, during presurgical monitoring a higher then normal rate of 0.15 seizures per hour was experienced by the patients [25]. Thus, an FPR_{max} equal to 0.15/hr is the maximum allowed false prediction rate for algorithm to be clinically viable.

Figure 2.4 captures the relationship between Seizure Prediction Horizon (SPH) and Seizure Occurrence Period (SOP) in relation to EEG time-profile.

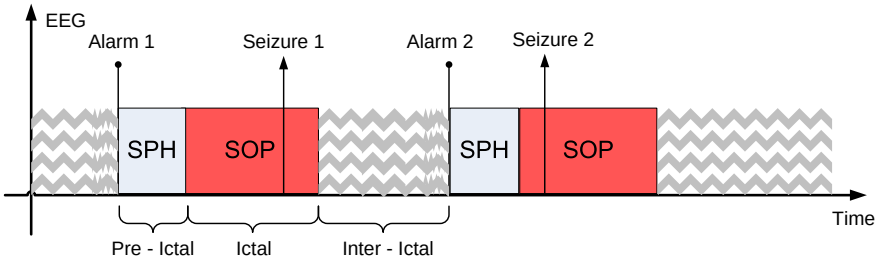

Figure 2.4: Seizure Prediction Variables

Sensitivity

The *sensitivity* is a single metric by which predictive performance of the algorithm is evaluated. Sensitivity depends on FPR_{max}, SOP, and SPH. It can be defined as simply the fraction of correct predictions over the total number of seizures [Appendix B].

The values of maximum seizure occurrence period SOP_{max}, minimum seizure prediction horizon SPH_{min}, and maximum false prediction rate FPR_{max} depend on a particular intervention system, which is, in general, not known at the time of evolution of seizure prediction algorithm. Therefore, sensitivity must be verified for a reasonable range of FPR_{max}, SPH, and SOP. The sensitivity of seizure prediction algorithm (S) is a function of the three variables:

$$S = f(FPR_{max}, SPH, SOP) \tag{2.6}$$

Thus, the FPR_{max}, SPH, and SOP must be reported along with the measure of sensitivity to fully characterize predictive performance of an algorithm.

It is important to mention that sensitivity (S) is in direct trade off with false prediction rate

(FPR): the parameters of seizure prediction method can be adjusted to improve sensitivity at the expense of increased false prediction rate and *vice versa*[4].

2.3.3 Prediction Methods

A prediction method along with characterizing measure form the core of seizure prediction algorithm. The method is representative of the properties of a seizure as evident through the change in characterizing measure. In this study, *two* simple prediction methods are used: *threshold* and *area* predictors. Both prediction methods are compared against a *random* predictor to observe whether a prediction is better than chance.

Threshold Predictor

A seizure can be viewed as hyper-synchronous neural activity. Therefore, characterizing index γ is expected to approach unity during the ictal EEG period. A drop in the value of γ can be used to differentiate between the pre-ictal and ictal stages of the seizure. Thus, a comparison of the index γ against a nominal (inter-ictal) threshold can be used to predict a prospective seizure.

The threshold τ is computed as follows:

$$\tau = \mu_{ij} - n_{ij} \times \sigma_{ij} \tag{2.7}$$

where μ_{ij} is the mean value of γ for a channel pair (i, j) computed in the *interictal* segment of the EEG, σ_{ij} is the *interictal* standard deviation of γ for the same period, and n_{ij} is the number of standard deviations below interictal mean required to achieve a certain prediction accuracy.

A seizure alarm is triggered when γ drops below the inter-ictal threshold, i.e. at the negative-slope crossings of the threshold τ. Any pair of channels (i, j) may trigger a prediction. Once the prediction is issued, no further alarms are allowed for a period equal to the *sum* of seizure prediction horizon (SPH) and seizure occurrence period (SOP).

[4]See Section 2.3.5 for discussion

Area Predictor

To reduce the number of false predictions caused by spikes in γ, an alternative predictor, based on accumulated *area*, can be used. This prediction method integrates γ below a fixed threshold and compares the result with inter-ictal reference area:

$$A_{curr} = \sum_{i=0}^{N-1} (\gamma[i] - \tau) \geq A_{ref} = K_{ij} \times \sigma_{ij} \tag{2.8}$$

where σ_{ij} is the standard deviation from inter-ictal mean, K_{ij} is adjustable integration period, and τ is an adjustable threshold below which the accumulation takes place. The threshold τ will have a different numerical value from the threshold detector, however, it is computed using the same formula.

Any pair of channels could trigger a seizure prediction. Once an alarm is issued, all accumulated areas are reset and any subsequent predictions are disabled for a period of time equal to the sum of (SPH) and (SOP).

Random Predictor

The random prediction method is used as a reference to assess the predictive significance of an algorithm. The output of the random predictor is independent of the EEG data. In order to compare the performance of threshold and area prediction methods to a random predictor, the common metric of *sensitivity*[5] is used. The expression for sensitivity of the random predictor is derived below.

To compute sensitivity of the random predictor, consider small *interictal* time period δ, and maximum false prediction rate FPR_{max}. Then, the probability of seizure prediction during *interictal* time interval δ is

[5]See Section 2.3.2 for definition of sensitivity

$$p = FPR_{max} \times \delta \tag{2.9}$$

Over a longer period of time T, the probability of at least one alarm is

$$P = 1 - (1 - FPR_{max} \times \delta)^{T/\delta} \tag{2.10}$$

Considering the limit of $\delta << T$ and the fact that

$$e = \lim_{x->\infty} (1 + \frac{1}{x})^x \tag{2.11}$$

We can approximate the probability P of at least one alarm as

$$P \approx 1 - e^{-FPR_{max}T} \tag{2.12}$$

Setting T equal to the seizure occurrence period SOP_{max}, yields the sensitivity of the random predictor.

2.3.4 Experimental Procedure

An experimental procedure was designed to handle the extensive EEG database and control the number of experimental variables to evaluate the predictive ability of phase synchronization algorithm. The experimental variables are identified in Table 2.5.

Variable	**Name**
Patients	Patient 1, Patient 2, Patient 3
Methods	Threshold, Area, Random
Electrodes	Number, Pairing
Sensitivity	FPR_{max}, SOP_{max}, SPH_{min}

Table 2.5: Experimental Variables

To limit the amount of computation, it is important to reduce the number of degrees of freedom

and choose a set that will be most useful in evaluating the sensitivity of phase synchronization algorithm. Thus, the experiment aims at, first, selecting the best algorithm-patient pair, and second, evaluating sensitivity of the chosen pair over a reasonable range of FPR_{max}, SOP_{max}, and SPH_{min}. The experimental procedure is divided into *two* main stages: *algorithm-patient selection* and *algorithm validation*.

Stage 1: Algorithm-Patient Selection

The purpose of the first stage is to select the highest-performing algorithm-patient pair which will be used to study the sensitivity of phase synchronization in the second stage of the experiment. The best-case scenario was chosen to study the *maximum possible* sensitivity given the current configuration of the algorithm. The choice can be justified by noting that, in each scenario, predictive performance is compared against the random predictor. Thus, all results are objectively evaluated against the common reference of the random predictor.

The following steps were used *for each patient* in the first stage:

1. Select a set of EEG electrodes
2. Compute the mean and standard deviation of interictal EEG segments
3. Configure sensitivity variables: FPR_{max}, SOP_{max}, and SPH_{min}
4. Run the algorithm and obtain first-pass results
5. Optimize threshold and area parameters
6. Iterate steps 4 and 5 until desired FPR_{max} is achieved
7. Tabulate the results
8. Repeat the steps above *for each prediction method*

Having completed stage 1 of the experiment, the best performing patient-predictor pair can be chosen based on maximum sensitivity. As a result of the first stage, the number of experimental variables is reduced to *three*: FPR_{max}, SOP_{max}, and SPH_{min}.

Stage 2: Algorithm Validation

The second stage evaluates the sensitivity of EEG phase synchronization algorithm. The sensitivity or TPR is determined by varying FPR_{max}, SOP_{max}, and SPH_{min} over a reasonable range. The range is captured in Table 2.6

Variable	Minimum	Average	Maximum	Units
SPH	16/60	5	10	minutes
SOP	10	30	50	minutes
FPR	0.08	0.15	0.3	seizures/hr

Table 2.6: Experimental Range of FPRmax, SOP, and SPH

First, the range of SPH was chosen based on the average value of 5 minutes, and the maximum and minimum deviations of 16 seconds and 10 minutes required for electrical stimulation and drug-release prevention systems respectively. Next, the range of SOP was selected around the average value of 30 minutes with a deviation of 10 and 50 minutes, which represent a more and less accurate prediction ability respectively. Finally, the range of FPR_{max} was chosen based on the minimum accepted value of 0.15/hr with the deviation of 0.08/hr and 0.3/hr that represent half and double the acceptable rate respectively. This range was used to construct the sensitivity plots presented in the Results Section 2.4.

2.3.5 Parameter Optimization

This section illustrates the trade-off between accuracy of the prediction (TPR) and the false prediction rate (FPR). Consider Figure 2.5, which shows a sample EEG signal beside the extracted characterization measure γ and thresholds *1* and *2*.

Notice that increasing the threshold level in Figure 2.5, increases the number of level crossings triggering a prediction. Thus, sensitivity of the algorithm improves at the expense of higher false prediction rate. In the extreme case of a continuous prediction, the algorithm will yield 100% sensitivity, however, the false prediction rate will be unacceptably high. Therefore, FPR_{max} must be reported along with the range of SPH and SOP for a valid assessment of algorithms' sensitivity.

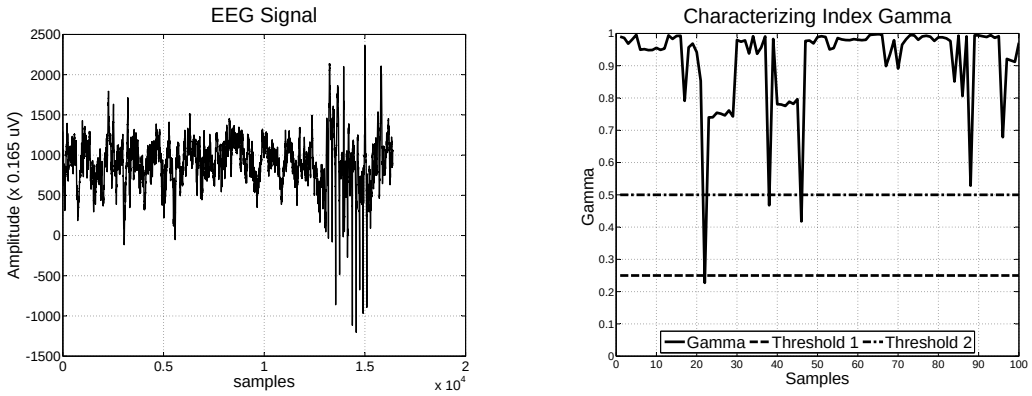

Figure 2.5: Parameter Optimization: TPR - FPR trade-off

2.4 Results

This section presents the experimental results for the *two* stages described in experimental procedure. The discussion of results is presented at the end of the section.

2.4.1 Stage 1: Selection

Table 2.7 displays the electrode pairings and interictal mean and standard deviation of γ for each patient.

Table 2.8 displays performance metrics[6] computed based on results of Table 2.7

Table 2.8 was obtained for each patient using a *fraction* of the total EEG recording. To achieve a target FPR of 0.15/hr, a recording of length $1/0.15 = 6.7$ hours is required with at least one seizure. Therefore, a recording period of over 6.7 hours was selected with an average of 3.3 seizures/patient [Table 2.9]. Note that the start and end samples in Table 2.9 refer to data samples in the EEG database [24].

For a fair comparison of sensitivity of different prediction methods, equal SPH, SOP, and FPR_{max} are required. While the values of SPH and SOP can simply be set prior to the experiment, it is not the case for FPR_{max}. To arrive at equal FPR_{max}, the threshold and reference area must be

[6]See Appendix B for metric definitions

Patient Number	Electrode Pairing	Interictal Mean of γ	Interictal STD of γ	FPR	SOP	SPH
1	$TBa_3 : TBb_3$	0.490	0.170	0.15/hr	30 min	5 min
	$TBa_3 : TBc_1$	0.496	0.164			
	$TLc_{15} : TLc_{16}$	0.494	0.170			
	$TLc_{16} : TLc_4$	0.495	0.170			
	$TLa_3 : TO_{12}$	0.494	0.169			
	$TO_{12} : TBa_2$	0.493	0.170			
	$TBa_2 : TBa_3$	0.487	0.171			
2	$TBa_1 : TBa_4$	0.873	0.182	0.15/hr	30 min	5 min
	$TBa_4 : TBb_1$	0.872	0.183			
	$TBb_1 : TBc_4$	0.869	0.183			
	$Gc_4 : Gb_4$	0.867	0.185			
	$Gb_4 : Gb_5$	0.867	0.187			
	$Gb_5 : Gc_5$	0.867	0.188			
3	$Hr_4 : Hr_5$	0.511	0.280	0.15/hr	30 min	5 min
	$Hr_1 : Hr_{10}$	0.512	0.275			
	$TOb_3 : TOb_4$	0.502	0.278			
	$TOb_4 : TOa_4$	0.502	0.285			
	$TOa_4 : TOc_1$	0.498	0.277			
	$TOc_1 : Hr_8$	0.501	0.278			
	$TOb_4 : TOb_1$	0.495	0.281			

Table 2.7: Experimental Data: Stage 1: Steps 1-3

No	Method	TP	FP	TN	FN	FPR	ACC	TPR	FPR/hr
1	Threshold	1	10	2.433	2	0.804	0.222	0.333	1.290
	Random	-	-	-	-	-	-	0.475	1.290
	Area	2	11	0.576	1	0.950	0.177	0.667	1.419
	Random	-	-	-	-	-	-	0.508	1.419
2	Threshold	1	9	5.140	2	0.636	0.358	0.333	1.029
	Random	-	-	-	-	-	-	0.402	1.029
	Area	1	0	14.14	2	0.000	0.883	0.333	0.000
	Random	-	-	-	-	-	-	0.000	0.000
3	Threshold	3	8	0.859	1	0.903	0.300	0.750	1.199
	Random	-	-	-	-	-	-	0.451	1.199
	Area	1	8	2.573	3	0.757	0.245	0.250	1.199
	Random	-	-	-	-	-	-	0.451	1.199

Table 2.8: Experimental Data: Stage 1: Steps 4-8

Patient	Start Sample	End Sample	Length	Number of Seizures
1	165994497	180744704	8 hrs	3
2	1	16589312	9 hrs	3
3	169365505	182269440	7 hrs	4

Table 2.9: Experimental Data: Stage 1: EEG dataset

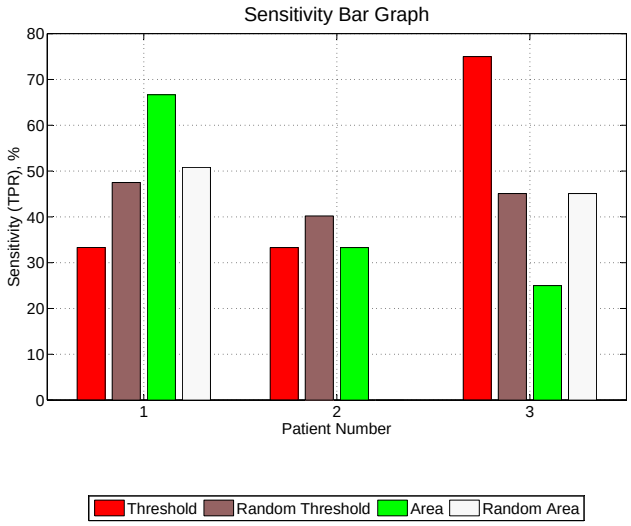

Figure 2.6: Experimental Data: Stage 1: Sensitivity Bar Graph

adjusted at each iteration until a near-equal FPR_{max} is achieved. The adjustment is more easily done to the reference area than in the case of a threshold predictor. The difficulty in realizing *exact* FPR_{max} is reflected in the variation of FPR in Table 2.8. Note that a zero FPR represents the case of a perfect prediction[7]. Therefore, rather than achieving an equal non-zero FPR_{max} for *Patient 2*, the opposite case was attempted.

A prediction method comparison based on sensitivity (TPR) data is presented in Figure 2.6. The red and dark-gray bars correspond to sensitivity based on threshold and its corresponding random predictor. Similarly, the green and light-gray bars represent the sensitivity of the area method and its corresponding random predictor.

Figure 2.6 shows that sensitivity of the random predictor is higher than the actual threshold and area predictors in half of the trials. In two-thirds of the trials, the area predictor outperformed its random match, whereas the threshold predictor was better than chance in one third of the trials. However, it is important to remember that dataset used in *Stage 1* is only a fraction of the total EEG recording for each patient. Thus, it is early to draw any conclusions on the usefulness of phase synchronization method until the *complete* dataset is examined in *Stage 2* of the experiment.

[7]See Appendix B for definition of perfect prediction

In order to complete *Stage 1*, we need to identify the best predictor-patient pair. Comparing the sensitivity (TPR) in Figure 2.6, we see 33% improvement of area predictor over threshold for *Patient 1*, equal performance for *Patient 2* and 55% improvement of threshold predictor over area for *Patient 3*. The advantage of area prediction over threshold is not clear and additional selection criteria is needed. Considering that area predictor produced an FPR of zero and the flexibility with which reference area may be adjusted to control FPR, the predictor based on accumulated area was selected for *Stage 2* of the experiment. Consequently, *Patient 2* was paired with the area predictor because their combined effect resulted in zero false prediction rate for *Patient 2*. Therefore, *Patient 2* and area predictor advance to *Stage 2* of the experiment.

2.4.2 Stage 2: Evaluation

The dependence of sensitivity (S) on the three variables SPH, SOP, and FPR_{max} introduced in Section 2.3.2 is explored in *Stage 2* of the experiment. The sensitivity is observed by holding two of the three variables constant, while varying the third. The results are tabulated and presented in the form of *three* 2-D plots of sensitivity S versus each of SPH, SOP, and FPR_{max}, and a 3-D ROC Curve[8] capturing the relationship between sensitivity and its fundamental trade-offs.

Dataset

The entire *Patient 2* dataset [Table 2.10] was used to examine the predictive ability of Phase Synchronization algorithm using accumulated area as a decision device.

Patient	Start Sample	End Sample	Length	Number of Seizures
2	1	55616512	30 hrs	10

Table 2.10: Experimental Data: Stage 2: EEG dataset

[8]See Appendix B on application of ROC curves to seizure prediction

Variation of Sensitivity with FPR

Table 2.11 shows the dependence of sensitivity (S) on false prediction rate (FPR), for a fixed SOP = 30 minutes and SPH = 5 minutes. Figure 2.7 shows how sensitivity varies with FPR, while keeping SPH and SOP constant.

FPR	TPR(Area)	TPR(Random)	SOP	SPH
0.000	0.333	0.000	30	5
0.375	0.400	0.171	30	5
0.784	0.500	0.324	30	5

Table 2.11: Experimental Data: Stage 2: TPR vs. FPR

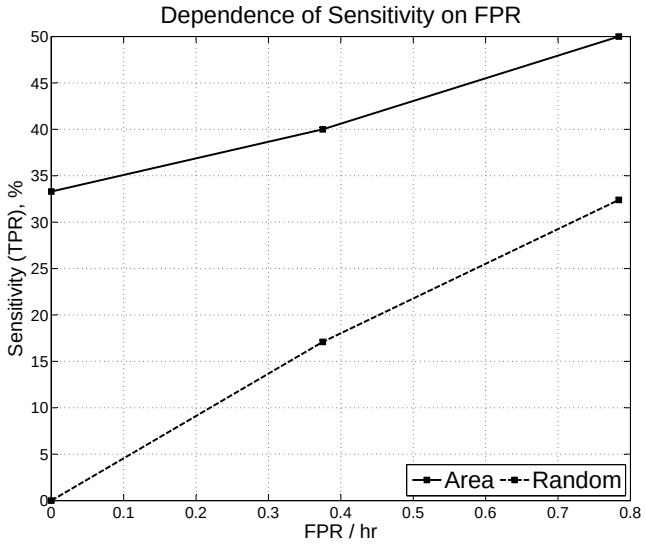

Figure 2.7: Sensitivity vs. FPR Plot

Variation of Sensitivity with SOP

Table 2.12 shows the dependence of sensitivity (S) on seizure occurrence period (SOP) for a fixed (SPH) = 5 minutes and an average $FPR_{max} = 0.568/hr$. Figure 2.8 shows how sensitivity (S) varies with SOP, while SPH and FPR are held constant.

SOP	TPR(Area)	TPR(Random)	FPR	SPH
10	0.200	0.132	0.852	5
30	0.400	0.180	0.613	5
50	0.600	0.264	0.239	5

Table 2.12: Experimental Data: Stage 2: TPR vs. SOP

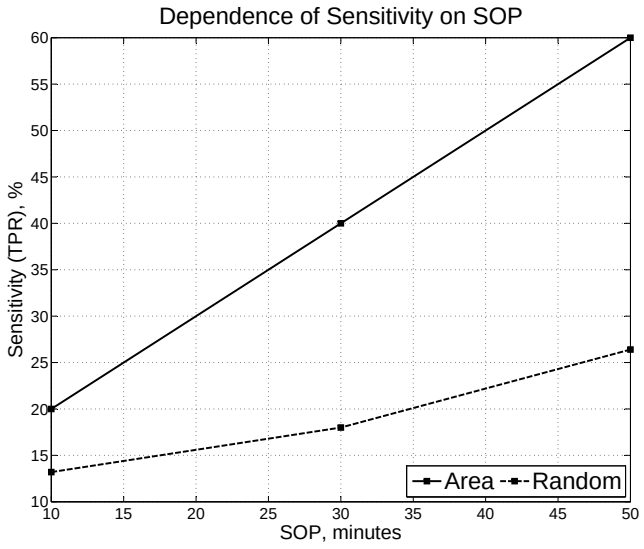

Figure 2.8: Sensitivity vs SOP Plot

Variation of Sensitivity with SPH

Table 2.13 summarizes the dependence of sensitivity (S) on seizure prediction horizon (SPH), for a fixed $SOP = SOP_{avg} = 30$ minutes and an average $FPR_{max} = 0.295/hr$. Figure 2.9 illustrates the dependence of sensitivity (S) on variation in SPH, while SOP and FPR are held constant.

SPH	TPR(Area)	TPR(Random)	FPR	SOP
16/60	0.571	0.138	0.296	30
5	0.400	0.112	0.239	30
10	0.300	0.161	0.351	30

Table 2.13: Experimental Data: Stage 2: TPR vs. SPH

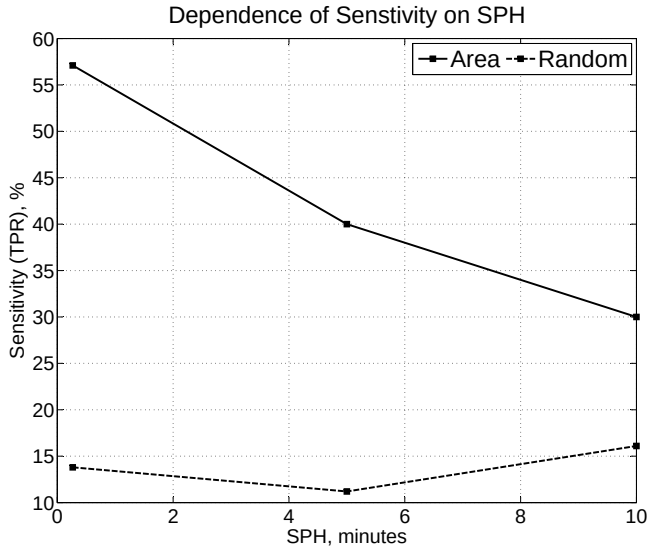

Figure 2.9: Sensitivity vs SPH Plot

ROC Plot

The data in Table 2.14 was used to construct the ROC plot[9] for phase synchronization algorithm employing area prediction method. Figure 2.10 shows how sensitivity S varies with both SOP and FPR_{max} for a fixed value of SPH equal to 5 minutes. (Note: The ROC data was interpolated by First Order Hold and fit by a 6th order polynomial. The original points are marked as squares in Figure 2.10)

[9]See Appendix B for application of ROC to seizure prediction

SOP	SPH	TPR	FPR
10	5	0.10	0.750
10	5	0.20	0.784
10	5	0.30	0.852
30	5	0.33	0.000
30	5	0.40	0.375
30	5	0.50	0.784
50	5	0.20	0.170
50	5	0.40	0.239
50	5	0.67	0.374

Table 2.14: Experimental Data: Stage 2: TPR vs SOP and FPR

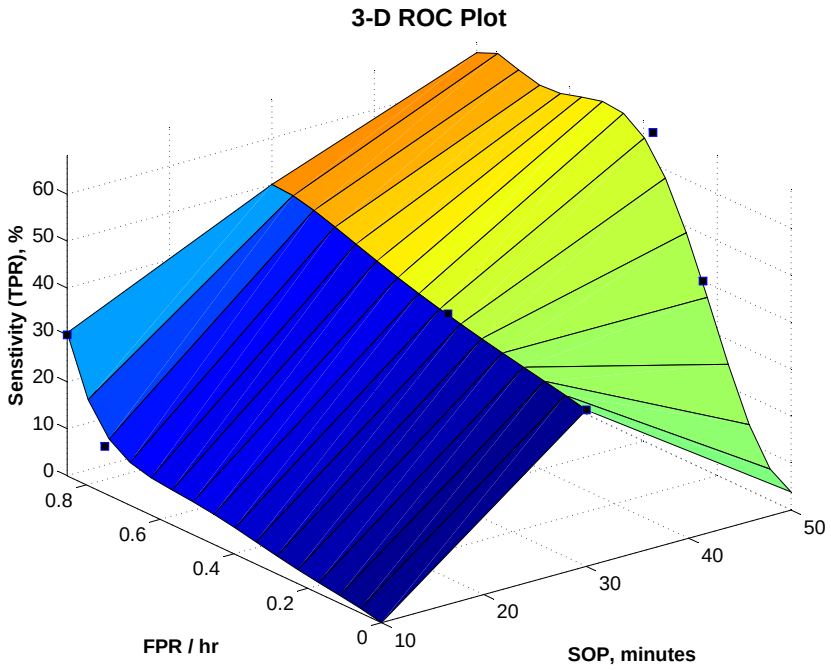

Figure 2.10: 3D Plot of Sensitivity vs SOP and FPR

2.4.3 Discussion

This section evaluates experimental results of *Stage 1* and *2* presented in Section 2.4. The discussion is structured in *two* parts: first, analysis and discussion of the selection *Stage 1* is presented, followed by discussion on sensitivity of the algorithm in *Stage 2*.

Discussion: *Stage 1*

Table 2.7 shows the inter-ictal mean μ_γ and standard deviation σ_γ used in computing the reference level for threshold and area predictors. The difference of μ across the *patients* suggests distinct levels of EEG synchronization. Although some variation in μ is expected due to differences in scope and types of seizures between each patient, a higher value of μ is observed for *Patient 2* in comparison with *Patients 1* and *3*. The reason for the higher inter-ictal mean may be explained by the severity of the condition for *Patient 2*. In addition, the time of day of the recording (i.e. the time of wake versus sleep), not reported with experimental data, could have an influence on EEG synchronization as found in [3]. To verify these hypotheses, additional patient data with similar diagnosis is required.

On the other hand, the value of μ across the *electrodes* for individual patients is nearly constant, with greatest variation for different electrode *types*. The differences between grid, strip, and depth electrodes are taken into account by computing statistics for *each* electrode separately. In this way, the prediction device is not biased to select a certain *type* of electrode over others.

An important set of experimental results is summarized in Table 2.8. This data was used to assess predictive performance of phase synchronization algorithm employing area and threshold prediction devices. Following the definitions in Appendix B, we can verify that:

- The sum of TP and FN is equal to the total number of seizures per patient
- The sum of TP, FP, TN, and FN is equal, within rounding error, for both area and threshold prediction methods
- The definitions for TPR, FPR, and accuracy (ACC) are consistent with experimental results in Table 2.8

The last *three* columns of Table 2.8 quantify predictive ability of the phase synchronization algorithm. Highest accuracy (ACC), lowest (FPR_{max}) and highest (TPR) are required for a successful prediction method. The highest accuracy of 88% and also the lowest FPR_{max} of zero is achieved by the area predictor for *Patient 2*. Considering the two false negative predictions in the same trial, the sensitivity (TPR) is only 33%. In contrast, the highest TPR in *Stage 1* is 75% achieved by the threshold predictor for *Patient 3* at the expense of non-zero $FPR = 1.199$ seizures/hr. The

superior performance of *Patient 2 - Area Predictor* pair is apparent from Table 2.8.

The bar chart in Figure 2.6 compares sensitivity (TPR) of each method with the model for random predictor introduced in Section 2.3.3. The comparison illustrates improvement in performance of area and threshold methods over the random predictor. Recall that sensitivity for the random predictor is defined by the following expression:

$$S \approx 1 - e^{-FPR_{max} \times SOP} \tag{2.13}$$

Because FPR_{max} could not be always made constant for area and threshold predictors, two different random models are associated with area and threshold methods. Figure 2.6 shows that in *3* out of *6* trials performed on *segmented* EEG recording, random predictor yielded higher sensitivity than area and threshold schemes. However, a *complete* EEG recording must first be examined before drawing a conclusion on predictive ability of the phase synchronization algorithm in its *current* configuration.

Discussion: *Stage 2*

This section discusses the central metric used to evaluate the seizure prediction algorithm: sensitivity. The dependence of sensitivity (S) on SPH, SOP, and FPR_{max} was introduced in Section 2.3.2. The results of *Stage 2* are interpreted below based on study of sensitivity as a function of SPH, SOP, and FPR_{max}.

Figure 2.7 illustrates a general increase in sensitivity associated with an increase in false prediction rate FPR_{max}. The data serves as an example of $TPR - FPR$ trade off presented in Section 2.3.5. Recall that any algorithm with FPR_{max} greater than 0.15/hr is not qualified for clinical application (Section 2.3.2). At exactly 0.15/hr, the sensitivity is around 36% for the area predictor. Even though the sensitivity of prediction based on area is 28% higher than that of random predictor, a sensitivity of 36% is not sufficient for medical application.

Consider the neighborhood point at $FPR = 0.375$, more than twice the required rate. This point

is defined by $TP = 4$, $FP = 11$, $TN = 35.9$, and $FN = 6$. We can calculate the probability P that given a positive prediction, the prediction is true:

$$P = \frac{TP}{TP + FP} = \frac{4}{4 + 11} \approx 0.27 \tag{2.14}$$

This calculation shows that at an FPR of double the clinically acceptable rate (0.15/hr), probability that our algorithm predicted the seizure correctly is only 27%. While area predictor is more sensitive to a prospective seizure than the random predictor, the value of sensitivity at clinically acceptable $FPR = 0.15/hr$ remains low.

Next, the influence of SOP on algorithm sensitivity is discussed. Figure 2.8 captures an increase in sensitivity, as a result of increasing SOP. This relation was anticipated because an expansion of SOP leads to a higher chance that a seizure will fall within expected occurrence period, thus increasing the number of true positives leading to increase in sensitivity. At an average acceptable SOP of 30 minutes, sensitivity of the algorithm was 40%, a 21% improvement over the random predictor.

The third variable examined in relation to sensitivity (S) is seizure prediction horizon (SPH). Higher sensitivity values are observed for lower SPH in Figure 2.9. These results deviate from the expected near-zero slope of S. A slope close to zero was expected because SPH affects both the numerator and denominator terms in the expression for sensitivity:

$$TPR = \frac{TP}{TP + FN} \tag{2.15}$$

The difference in expected and actual results can be explained by noting the variation in FPR across the data points. This difference in FPR causes the sensitivity predicted by area and random methods to deviate from its expected value.

The ROC plot shown in Figure 2.10 provides a visual way of understanding the limits of performance placed on sensitivity by SOP and FPR_{max}. Consistent with Figures 2.7 and 2.8, an

increase in either SOP or FPR_{max} causes sensitivity to increase. The highest sensitivity achieved for the current configuration and experimental space of the algorithm is 67%. This is 40% above the sensitivity at critical $FPR = 0.15$/hr.

Results obtained in this experiment are comparable to a parallel study [26], in which the *same* EEG database was used to evaluate sensitivity as a function of SPH, SOP, and FPR for a different non-linear characterizing measure. The sensitivity of 37% at maximum tolerable $FPR = 0.15$/hr and $SOP = 30$ minutes as shown in the ROC plot suggests the need to improve current configuration of the algorithm. The next Section 2.4.4 on *Future Work* proposes a list of possible improvements.

2.4.4 Future Work

This section provides a list of improvements to *current* configuration of EEG phase synchronization algorithm. The following *future work* items are identified:

Signal Processing

1. *EEG Frequency Bands.* The data reported in [19] suggests that pre-ictal changes in phase synchronization are dominant in the β band. Thus, additional insight can be gained by filtering EEG signal into its frequency bands: $\delta \in$ [0.5 - 4]Hz, $\theta \in$ [4 - 8]Hz , $\alpha \in$ [8 - 13]Hz, $\beta \in$ [13 - 30]Hz, $\gamma \in$ [30 - 48]Hz.

2. *Windowing Function.* To achieve higher accuracy due to windowing of the sampled EEG signals, a different windowing function such as Hanning window can be used in place of rectangular window.

3. *Window Overlap.* To smooth out edge effects due to windowing and reduce spikes in the time profile of γ, consecutive windows can be designed to overlap by a certain percentage.

Methodology

1. *Algorithm Comparison.* To verify reported similarity between EEG phase synchronization and comparable measures such as Maximum Linear Cross-Correlation [6] and Dynamical

Similarity Index [19], the alternative algorithms may be implemented to ascertain their predictive performance.

2. *Balanced Evidence.* To make sure that future study is not based heavily on the research work of Seizure Prediction Group in Freiburgh University and the University Hospital but strengthened through evidence from other sources.

3. *Correction of Artifacts.* To eliminate adverse influence of artifacts on EEG prediction measure, artifacts such as eye-movement and the wake versus sleep states of the patient, must be identified and addressed in the prediction algorithm.

4. *Improved Implementation.* By implementing the entire algorithm in C will help speed up the computation as well as avoid potential timing errors due to repeated execution of Matlab and C.

2.5 Conclusions

EEG phase synchronization algorithm was selected based on its potential for predicting prospective seizures and ease of on-chip implementation. A comprehensive procedure was used to evaluate the performance of the algorithm on a continuous, long-term EEG recording. The results of the experiment indicate a sensitivity of 37% at FPR_{max} of 0.15/hr and SOP of 30 minutes. The algorithm performed 30% better than the random predictor. A sensitivity of 37% at $FPR_{max} = 0.15$/hr suggests the need to improve the current configuration of the algorithm. The future work section proposes a list of improvements in signal processing and methodology.

Chapter 3

Implementation

3.1 Matlab Implementation

3.1.1 Introduction

This section presents Matlab implementation of the phase synchronization algorithm. Section 3.2.3 provides a top level overview of the model. Section 3.2.3 examines implementation of *two* main signal processing blocks. Verification of the model is presented in Section 3.1.3

3.1.2 Functional Overview

Top Level

Figure 3.1 shows system-level Matlab implementation of the phase synchronization algorithm.

The model in Figure 3.1 consists of EEG reader written in C (provided with EEG database [24]), and seizure prediction algorithm implemented in Matlab. The top-level *Matlab* script directs the execution of EEG reader and the algorithm.

Top-level implementation can be summarized as follows:

- Initialize patient parameters
- For each window of EEG data:
    1. Execute EEG Data Reader

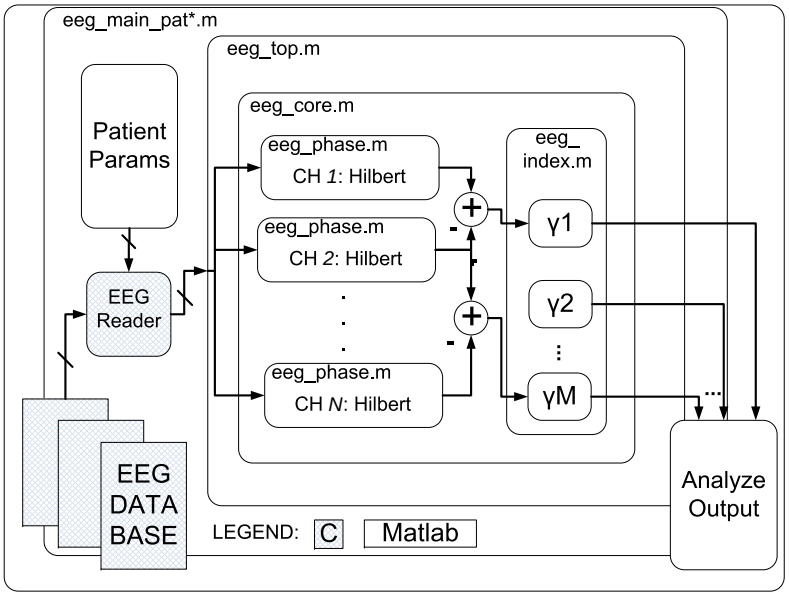

Figure 3.1: Matlab Implementation Overview

2. Compute synchronization index γ
3. Form a prediction based on γ

- Plot ROC

Effort was made to make Matlab implementation as modular as possible in order to simplify debugging and hardware implementation.

Block Level

At the block level, signal processing pipeline consists of *two* main functional blocks: Hilbert transformer and γ computational block.

Hilbert Transformer Hilbert transformer is approximated by Direct Form FIR filter of 64th order. The filter is designed for a sampling frequency of 512 Hz and implemented using equirriple approximation method. Coefficients of Hilbert transformer are quantized to 16 bits fixed point and scaled to utilize full dynamic range. Figure 3.2 shows a superposition of magnitude and frequency response of *FIR approximation* of Hilbert Transformer[1].

[1]See Appendix A for discussion on Hilbert Transform

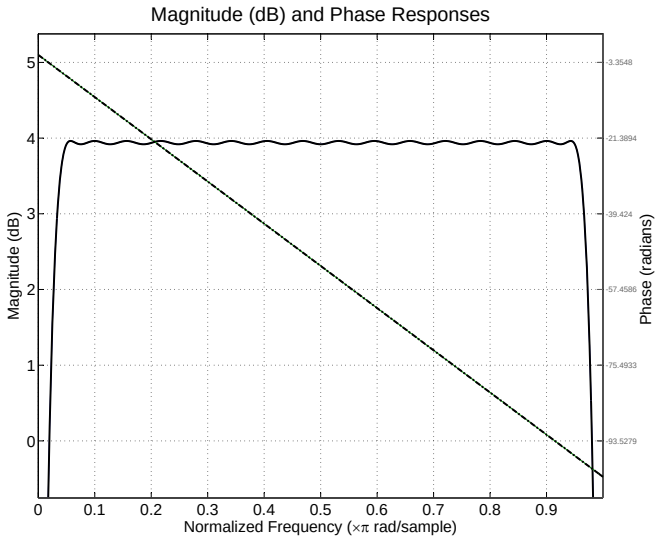

Figure 3.2: Hilbert Transformer FIR Approximation: Magnitude and Phase Response

Synchronization Index Computational block of synchronization index γ implements the equation derived in Section 2.2.2, repeated here for convenience:

$$\gamma = \frac{1}{N}\sqrt{(\sum_{k=0}^{N-1}\cos\phi_{xy}(kT))^2 + (\sum_{k=0}^{N-1}\sin\phi_{xy}(kT))^2} \tag{3.1}$$

3.1.3 Verification

To verify the operation of each functional block and system as a whole, a series of block and top-level tests were designed. In the following discussion, the results of *single-tone* and *multi-tone* tests of the Hilbert transformer are presented.

Figure 3.3 shows the output of FIR approximation of Hilbert transformer for a given sinusoidal input.

Observe the delay of $\pi/2$ and the change in amplitude due to windowing and gain of the Hilbert transformer in Figure 3.3.

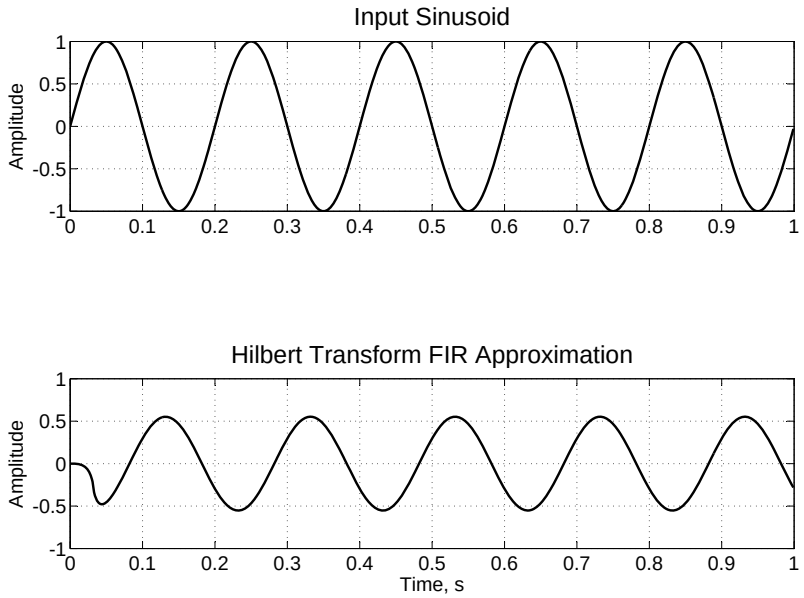

Figure 3.3: Hilbert Transformer FIR Approximation: Sinusoidal Input

Figure 3.4 shows the output of Hilbert transformer in response to a square wave input. The figure compares *Matlab* and *DSP platform* implementations. The FIR approximation to Hilbert transformer was implemented on TMS320C6713 DSP Starter Kit (DSK) [9].
Figure 3.4 shows a close resemblance between Matlab and DSP outputs for a square wave input.

Figure 3.5 compares the outputs of Hilbert transformer for a multi-tone EEG signal input.

The outcomes of *single-tone* and *multi-tone* Hilbert transformer tests are consistent with expected results.

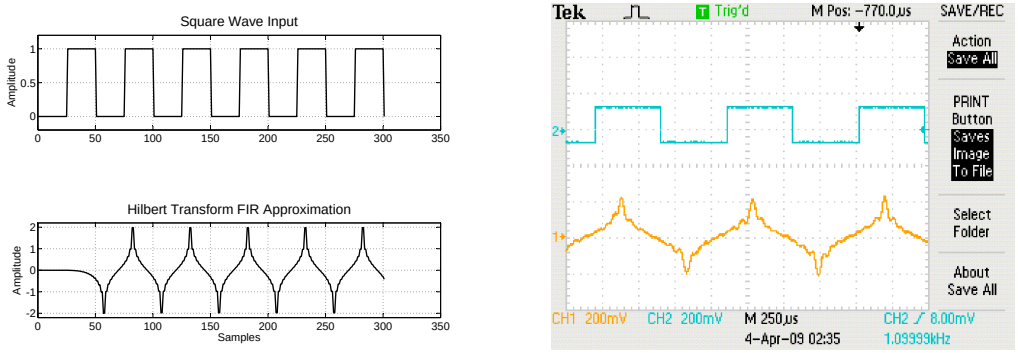

Figure 3.4: Hilbert Transformer FIR Approximation: Square Wave Input

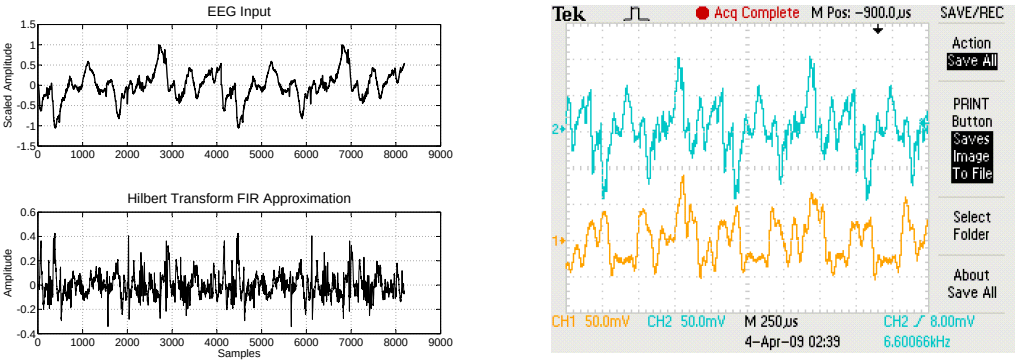

Figure 3.5: Hilbert Transformer FIR Approximation: EEG Input

3.2 FPGA Implementation

3.2.1 Introduction

This section proposes FPGA implementation of EEG phase synchronization algorithm. Section 3.2.2 identifies implementation constraints and selects fitting FPGA technology. Section 3.2.3 provides the top level perspective and proposes block level implementation. The section concludes by summarizing the results.

3.2.2 Technology Selection

Two main constraints were identified in selecting FPGA technology for algorithm implementation: *signal processing IP* and *I/O Interface*. Given the low-frequency nature of EEG signals ($F_s = 512$ Hz), constraint on FPGA speed is relaxed. The following technology options were considered (Table 3.2)

Board Name	**FPGA**	**Relevant IO**	**Relevant IP**
XUPV5	Virtex-5 XC5VLX110T	RS-232 (x2)	DSP 48E
XUPV2P	Virtex-II Pro XC2VP30	RS-232	FFT, IFFT, FIR, DFPSQRT
Spartan-3E	Spartan-3E XC3S500E	RS-232 (x2)	Multiplier Blocks

Table 3.1: Technology Selection: FPGA Board

As shown in Table 3.2, XUPV2P30 Virtext II board [28] was chosen for algorithm implementation.

3.2.3 Functional Overview

Top Level

EDK Base System Builder was used in board-level implementation of the phase synchronization algorithm. The system includes the following building blocks:

Board Name	FPGA	IO Interface	IP Cores
XUPV2P	Virtex-II Pro XC2VP30	RS-232	Phase Synchronization Algorithm Sine Cosine Look Up Table DFPSQRT CORDIC

Table 3.2: Technology Selection: FPGA Board

Block Level

Figure 3.6 shows the proposed FPGA implementation of the algorithm. As described in Section 2.2.2, in addition to $s(\tilde{t})$, the Hilbert Transformer, the following functions must be implemented in hardware: $\arctan(x)$, $\sqrt{x}$, $\sin(x)$, and $\cos(x)$.

Hilbert Transformer Hilbert transformer is realized by a Direct Form FIR filter in Fully Parallel architecture with 64-taps.

Square Root Digital floating point square root (*DFPSQRT*) IP [27] is used to implement the square root function. *DFPSQRT* IP is IEEE-754 compliant, utilizes 4 pipelines and supports single precision format.

Trigonometric Functions $\sin(x)$ and $\cos(x)$ are implemented with 10 bit in, 32 bit out *Sine Cosine Look Up Table* using block ROM [27].

*CO*ordinate *R*otation *DI*gital *C*omputer (*CORDIC*) algorithm is used to perform the $\arctan(x)$ function. CORDIC algorithm [29] provides an iterative approximation of $\arctan(x)$ using shift and

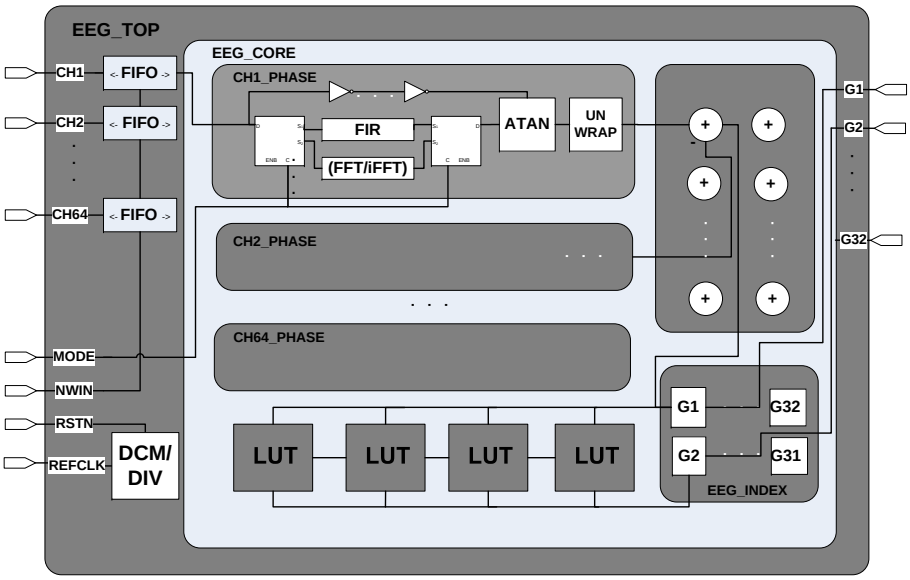

Figure 3.6: FPGA Implementation Overview

add operations.

Comparable FPGA implementation is presented in [12].

3.3 Conclusions

In this section Matlab model and proposed FPGA implementation have been described. The Matlab model was written in a modular form to simplify debugging and hardware implementation. The operation of its main functional blocks was verified in Matlab and TMS320C6713 DSP Starter Kit (DSK) [9]. The results obtained show similarity between the simulated model and its implementation. An FPGA architecture was proposed. Xilinx Virtex-II Pro was selected for implementation of the algorithm. The use of $CORDIC$ algorithm and FPGA IP addressed the computational complexity of γ.

Chapter 4

Conclusions

Research in seizure prediction is an international effort in search for a reliable prediction method that can meet the standards of clinical application. Only recently first attempts were made to study *causal* seizure prediction schemes. Nevertheless, sound methodology exists in addition to hours of continuous, long-term EEG recordings. These conditions set up a favorable environment for research in seizure prediction.

In this study, EEG phase synchronization algorithm was selected and evaluated on a dataset of *three* patients for a total of 230 hours of EEG and 30 seizures. The results of the study indicate the best case sensitivity of 37% at $FPR_{max} = 0.15$/hr and $SOP = 30$ minutes. While this sensitivity is 30% higher than that of a random predictor, it is not sufficient for clinical application. The sensitivity of 37% suggests the need to improve current configuration of the algorithm. A list of improvements was proposed in Section 2.4.4.

The algorithm was implemented and verified in Matlab via top and block-level tests in addition to TMS320C6713 DSP Platform [9]. Virtex-II technology was selected for FPGA implementation. An architectural overview and implementation of main functional blocks was proposed.

Bibliography

[1] Wolf A, Swift JB, Swinney L, and Vastano A. Determining lyapunov exponents from a time series. *Physica D*, 16:285–317, 1985.

[2] Stein AG, Eder HG, Blum DE, Drachev A, and Fisher RS. An automated drug delivery system for focal epilepsy. *Epilepsy Res*, 39:103–114, 2000.

[3] Schelter B, Winterhalder M, and Maiwald T et. al. Do false predictions of seizure depend on the state of vigilance? a report from two seizure-prediction methods and proposed remedies. *Epilepsia*, 47:2058–2070, 2006.

[4] Roland E. Best. *Phase-Locked Loops: Design, Simulation, and Applications*. McGraw-Hill, 2003.

[5] Mormann F, Andrzejak R, Elger C, and Lehnertz K. Seizure prediction: the long and winding road. *Brain*, 130:314–333, 2007.

[6] Mormann F, Andrzejak RG, and Kreuz T. Automated detection of a preseizure state based on a decrease in synchronization in intracranial electroencephalogram recordings from epilepsy patients. *Physical Review*, 67:021912–021912, 2003.

[7] Mormann F, Kreuz T, and Rieke C. On the predictability of epileptic seizures. *Journal of Clinical Neurophysiology*, 116:569–587, 2005.

[8] Osterhage H, Mormann F, and Staniek M. Measuring synchronization in the epileptic brain: A comparison of different approaches. *International Journal of Bifurication and Chaos*, 17:3539–3544, 2007.

[9] Texas Instruments. Tms320c6713 dsp starter kit (dsk), April 2009. Available from http://focus.ti.com/.

[10] Aziz J, Karakiewicz R, Genov R, Chiu AWL, Bardakjian BL, Derchansky M, and Carlen PL. In vitro epileptic seizure prediction microsystem. *IEEE International Symposium on Circuits and Systems ISCAS*, pages 3115–3118, 2007.

[11] Bauer J and Burr W. Course of chronic focal epilepsy resistant to anticonvulsant treatment. *Seizure*, 10:239–246, 2001.

[12] Jones JD, Pei JS, and Tull MP. Embedded algorithms within an fpga-based system to-process nonlinear time series data. *Conference on Sensors and Smart Structures Technologies for Civil, Mechanical, and Aerospace Systems*, 6932:I9323–I9323, 2008.

[13] Annegers JF. *The epidemiology in epilepsy.* Baltimore: Williams and Wilkins, 1996.

[14] Lehnertz K, Mormann F, and Osterhage H. State-of-the-art of seizure prediction. *Journal of Clinical Neurophysiology*, 24:147–153, April 2007.

[15] Lehnertz K, Andrzejak RG, and Arnhold J. Nonlinear eeg analysis in epilepsy: Its possible use for interictal focus localization, seizure anticipation, and prevention. *Journal of Clinical Neurophysiology*, 18:209–222, 2001.

[16] Mardia KV. *Probability and Mathematical Statistics: Statistics of Directional Data.* Academic Press, 1972.

[17] Iasemidis LD, Shiau DS, and Chaovalitwongse W. Adaptive epileptic seizure prediction system. *Clinical Neurophysiology*, 116:506–516, 2005.

[18] D'Alessandro M, Vachtsevanos G, and Esteller R. A multi-feature and multi-channel univariate selection process for seizure prediction. *Clinical Neurophysiology*, 116:506–516, 2005.

[19] Le Van Quyen M, Soss J, and Navarro V. Preictal state identification by synchronization changes in long-term intracranial eeg recordings. *Clinical Neurophysiology*, 116:559–568, 2005.

[20] Morrell M. Brain stimulation for epilepsy: can scheduled or responsive neurostimulation stop seizure. *Current Opinion in Neurology*, 19:164–168, 2006.

[21] Brodie MJ and Dichter MA. Drug therapy - antiepileptic drugs. *New England Journal of Medicine*, 334:168–175, 1996.

[22] Alan V. Oppenheim and Ronald W. Schafer. Prentice Hall, 1998.

[23] World Health Organization. Epilepsy fact sheet, January 2009. Available from www.who.int.

[24] International Seizure Prediction Project. Eeg database, April 2009. Available from https://epilepsy.uni-freiburg.de/.

[25] Haut SR, Swick C, Freeman K, and Spencer S. Seizure clustering during epilepsy monitoring. *Epilepsia*, 43:711–716, 2002.

[26] Maiwald T and Winterhalder M et. al. Comparison of three nonlinear seizure prediction methods by means of the seizure prediction characteristic. *Physica D*, 194:357–368, 2004.

[27] Xilinx. Virtex-ii pro fpga user guide, Nov 2007. Available from http://www.xilinx.com/.

[28] Xilinx. Virtex-ii pro development system, April 2009. Available from http://www.xilinx.com/.

[29] Hu YH. Cordic - based vlsi architectures for digital signal processing. *IEEE Signal Processing Magazine*, 1992.

Appendix A

Appendix A

A.1 Hilbert Transform

A.1.1 Introduction

A discrete time signal can be represented in the frequency domain by its Discrete Time Fourier Transform (DTFT). In general, complete knowledge of magnitude and phase for all frequencies $-\pi < \omega \leq \pi$ is required to completely specify a signal in time domain. However, additional information about the signal induces certain properties on DTFT. For example, for a real $x[n]$, its discrete-time Fourier transform is conjugate symmetric: $X(e^{j\omega}) = X^*(e^{-j\omega})$ Thus, to completely specify $x[n]$, it is sufficient to specify $X(e^{j\omega})$ for only the positive frequencies $0 < \omega \leq \pi$. In case of Hilbert transform, the *causality* of the sequence implies a relationship between the real and imaginary parts of DTFT.

A.1.2 Hilbert Transform Relationship

Since we are interested in relating the real and imaginary parts of DTFT, one-sided condition will be applied to the discrete-time Fourier transform. Thus, we consider a causal sequence for which DTFT is zero over the bottom half of the unit circle

$$X(e^{j\omega}) = 0, \qquad -\pi \leq \omega < 0 \tag{A.1}$$

The sequence $x[n]$ corresponding to $X(e^{j\omega})$ must be complex, since, if $x[n]$ were real, the DTFT would be conjugate symmetric, violating the above condition. Therefore, we express $x[n]$ as a sum

$$x[n] = x_r[n] + jx_j[n] \tag{A.2}$$

where $x_r[n]$ and $x_j[n]$ are real sequences. Let $X_r(e^{j\omega})$ and $X_j(e^{j\omega})$ denote the DTFT of the real sequences $x_r[n]$ and $x_j[n]$, then

$$X(e^{j\omega}) = X_r(e^{j\omega}) + jX_j(e^{j\omega}) \tag{A.3}$$

Expressing the real and imaginary parts of DTFT in terms of $X(e^{j\omega})$ and its conjugate $X^*(e^{-j\omega})$, we obtain

$$X_r(e^{j\omega}) = \frac{1}{2}[X(e^{j\omega}) + X^*(e^{-j\omega})] \tag{A.4}$$

and

$$jX_j(e^{j\omega}) = \frac{1}{2}[X(e^{j\omega}) - X^*(e^{-j\omega})] \tag{A.5}$$

Note that $X(e^{j\omega})$ is zero for $-\pi \leq \omega < 0$, thus, there is no overlap between the nonzero portions of $X(e^{j\omega})$ and $X^*(e^{-j\omega})$. Therefore, $X(e^{j\omega})$ can be fully recovered from either $X_r(e^{j\omega})$ or $X_j(e^{j\omega})$:

$$\begin{aligned} X(e^{j\omega}) &= 2X_r(e^{j\omega}), && 0 \leq \omega < \pi \\ &= 0, && -\pi \leq \omega < 0 \end{aligned} \tag{A.6}$$

and

$$\begin{aligned} X(e^{j\omega}) &= 2jX_j(e^{j\omega}), \qquad 0 \leq \omega < \pi \\ &= 0, \qquad -\pi \leq \omega < 0 \end{aligned} \tag{A.7}$$

Therefore, $X_r(e^{j\omega})$ and $X_j(e^{j\omega})$ can be directly related by

$$\begin{aligned} X_j(e^{j\omega}) &= -jX_r(e^{j\omega}), \qquad 0 \leq \omega < \pi \\ &= jX_r(e^{j\omega}), \qquad -\pi \leq \omega < 0 \end{aligned} \tag{A.8}$$

or

$$X_j(e^{j\omega}) = H(e^{j\omega})X_r(e^{j\omega}) \tag{A.9}$$

where

$$\begin{aligned} H(e^{j\omega}) &= -j, \qquad 0 < \omega < \pi \\ &= j, \qquad -\pi < \omega < 0 \end{aligned} \tag{A.10}$$

Thus, one-sided property of DTFT induced the relationship $H(e^{j\omega})$ between the real and imaginary parts of discrete-time Fourier transform. Relationships of this type between the real and imaginary parts of complex functions are commonly known as *Hilbert transform relationships*.

The Hilbert transform $H(e^{j\omega})$ is an ideal 90-degree phase shifter. It has unity magnitude and a phase angle of $-\pi/2$ for $0 < \omega < \pi$ and $\pi/2$ for $-\pi < \omega < 0$. As a result, $x_i[n]$ can be obtained by processing $x_r[n]$ with an LTI discrete-time system, with frequency response $H(e^{j\omega})$.

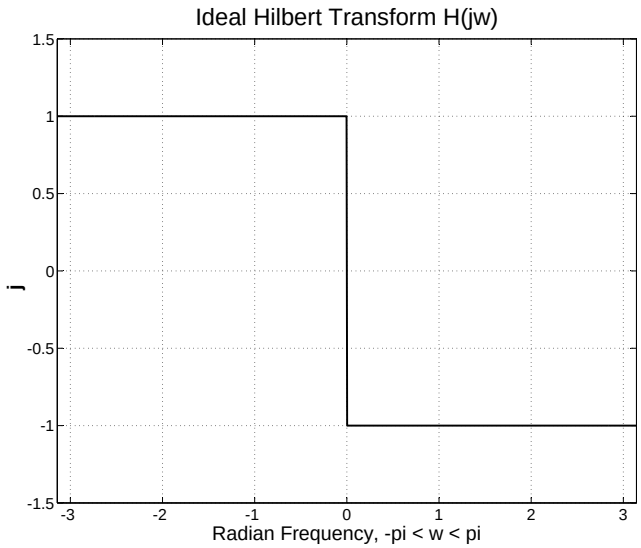

Figure A.1: Ideal Hilbert Transform Frequency Response

The corresponding impulse response $h[n]$ in time domain can be derived as follows:

$$\begin{aligned} h[n] &= \frac{1}{2\pi}\int_{-\pi}^{\pi} H(e^{j\omega})e^{j\omega n}d\omega \\ &= \frac{1}{2\pi}\int_{-\pi}^{0}(je^{j\omega n}d\omega) - \frac{1}{2\pi}\int_{0}^{\pi}(je^{j\omega n}d\omega) \end{aligned} \tag{A.11}$$

or

$$\begin{aligned} h[n] &= \frac{2}{\pi}\frac{\sin^2(\pi n/2)}{n}, \qquad n \neq 0 \\ &= 0, \qquad\qquad\qquad\quad n = 0. \end{aligned} \tag{A.12}$$

A.2 FIR Approximation of Hilbert Transform

The Hilbert Transform represents an *ideal* 90-degree phase shifter. Its frequency response,

$$H(e^{j\omega}) = \sum_{n=-\infty}^{\infty} h[n]e^{-j\omega n} \tag{A.13}$$

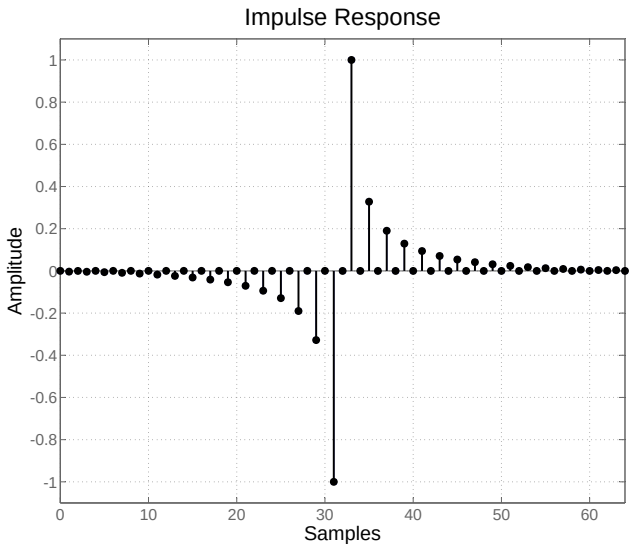

Figure A.2: Impulse Response of FIR Approximation to Hilbert Transform Order 64

is not absolutely summable and converges only in the mean-square sense. Thus, in practical design, *approximations* to the ideal Hilbert Transform are obtained.

An FIR approximation with *linear phase* can be designed using either the window method or the equiripple approximation method. In such implementation, the 90-degree phase shift is realized exactly in addition to linear phase component of the FIR filter. Therefore, a multi-tone signal will have *different* amounts of delay added to its constituent frequency components when filtered by FIR *approximation* of the Hilbert Transform.

Recall, the definition for instantaneous phase in Section 2.2.2:

$$\phi(t) = \arctan(\frac{\tilde{s(t)}}{s(t)}) \tag{A.14}$$

Define the difference in instantaneous phase $\phi(t)$ for two EEG time windows x and y at time kT as $\phi_{xy}(kT)$. Then, $\phi_{xy}(kT)$ measures the difference in phase content of the present frequency components in the two EEG time windows. A value of $\phi_{xy}(kT)$ equal to zero suggests equal amount of delay at each frequency in the EEG spectrum of windows x and y, while the magnitude of non-zero $\phi_{xy}(kT)$ phase difference determines the amount of asynchronicity of the two EEG window profiles.

Therefore, an extension of definition of instantaneous phase from a set of complex numbers to a set of non-linear time series over a finite length is justified in its ability to measure amount of synchronization of a pair of signals.

Appendix B

Appendix B

B.1 ROC: Receiver Operating Characteristic

Receiver operating characteristic (ROC) is a binary classifier system adopted from signal detection theory as a method for evaluating performance of a binary classification algorithm such as one used to predict a seizure. The ROC can be represented as a plot of *sensitivity* (TPR) versus the *false prediction rate* (FPR) of the algorithm.

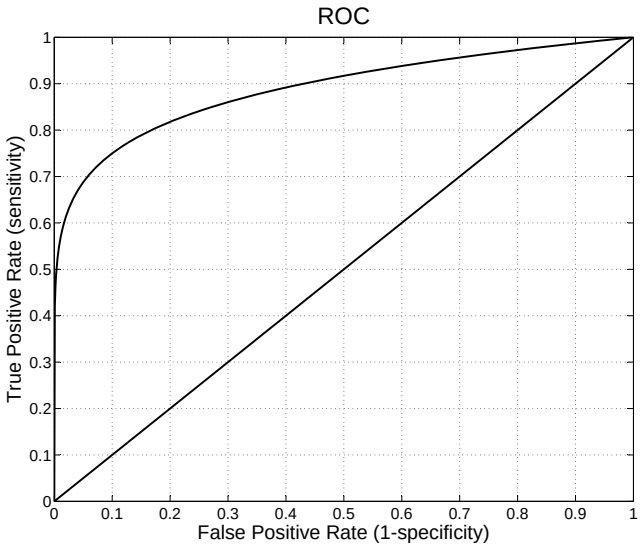

Figure B.1: Reciever Operating Characteristic (ROC) Plot

The sensitivity of a seizure prediction algorithm is equivalent to true positive prediction rate (TPR). While $(1 - specificity)$ is equal to the false prediction rate (FPR) [1].

To appreciate the role of ROC in algorithm evaluation, it is important to grasp the fundamental rates: TPR and FPR.

B.1.1 Fundamental Definitions

Consider a binary classification problem, in which the outcomes are labeled as either positive $[p]$ or negative $[n]$. There are four possible outcomes of a binary classifier.

Given the actual outcome of a binary event is $[p]$, if the predicted outcome is also $[p]$, the prediction is classified as a *true positive* (TP). In the case of prediction value equal to $[n]$, the prediction is classified as a *false negative* (FN). Similarly, given the actual outcome of an event is $[n]$, if the predicted outcome is $[n]$, the prediction is considered a *true negative* (TN). In the opposite case, when the predicted outcome is equal to $[p]$, the prediction is classified as a *false positive* (FP). The results can be grouped in the form of a 2x2 *confusion matrix*, also known as *contingency table*.

	Actual Positive	**Actual Negative**
Predicted Positive	TP	FP
Predicted Negative	FN	TN

Table B.1: Confusion Matrix

Having defined the fundamental variables, we can extract useful performance information by considering their ratios. An ROC curve is defined in terms of TPR (sensitivity) and FPR (1-specificity).

$$TPR = \frac{TP}{P} = \frac{TP}{TP + FN} \tag{B.1}$$

[1] See Section 2.3.2 for application of TPR and FPR in seizure prediction

$$FPR = \frac{FP}{N} = \frac{FP}{FP + TN} \tag{B.2}$$

where P and N stand for the total number of positive and negative outcomes respectively. TPR determines the number of correctly predicted positive instances among *all* positive occurrences of the event. Similarly, FPR quantifies the number of incorrect positive predictions among *all* negative occurrences (i.e. non-occurrences) of the event.

Other useful ratios in measuring predictive performance of the algorithm are *accuracy* (ACC), *specificity* (SPC), *positive predictive value* (PPV), and *negative predictive value* (NPV).

$$ACC = \frac{TP + TN}{P + N} = \frac{TP + TN}{TP + TN + FP + FN} \tag{B.3}$$

$$SPC = \frac{TN}{N} = \frac{TN}{FP + TN} = 1 - FPR \tag{B.4}$$

$$PPV = \frac{TP}{TP + FP} \tag{B.5}$$

$$NPV = \frac{TN}{TN + FN} \tag{B.6}$$

The accuracy ratio evaluates the number of correct positive *and* negative, predictions over the entire sample space. The specificity considers the ratio of correctly predicted true negatives over the *total* number of negative occurrences. Finally, the positive and negative prediction values quantify the probability that either a positive (PPV) or negative (NPV) prediction is correct.

B.1.2 ROC Space

Having defined the fundamental variables and ratios, we can now see how they work in application to ROC plot used to evaluate predictive ability of a binary classification algorithm.

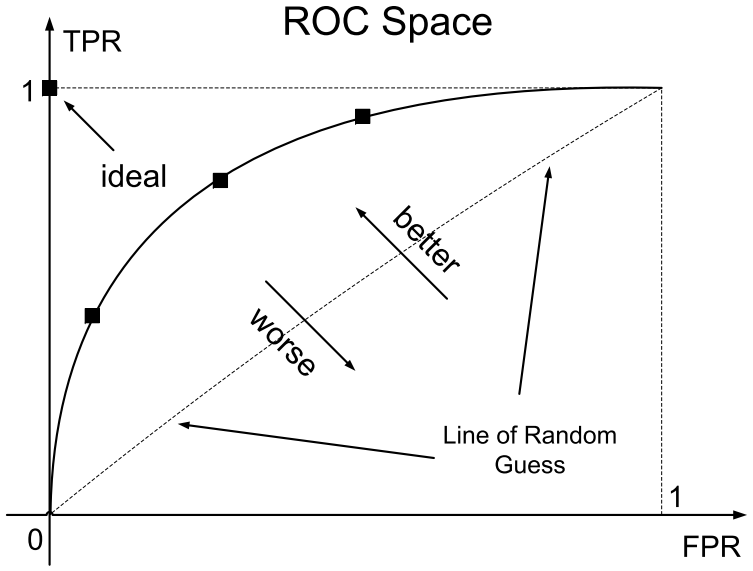

Figure B.2: ROC Space

The *ROC* space is defined in terms of TPR and FPR two trade-off quantities: true positive predictions (benefits) and false positive predictions (costs). Since TPR is equivalent to *sensitivity* and FPR is equal to $(1 - specificity)$, the *ROC* plot is often referred to as *sensitivity* vs $(1 - specificity)$ plot. One point on the *ROC* curve represents a single instance of the 2×2 confusion matrix (Table B.1).

To gain an intuitive feel for *ROC* space, consider the ideal case of a *perfect prediction* in the top-left corner of the ROC plot: $(FPR, TPR) = (0, 1)$. This point denotes 100% sensitivity (no false negatives) and 100% specificity (no false positives). The $(0, 1)$ point is called a *perfect classification*. Its opposite is located at the bottom-right corner $(FPR, TPR) = (1, 0)$ corresponding to 0% correct and 100% incorrect predictions. In the case of a random prediction, the outcome is expected to lie along the diagonal line $TPR = FPR$, known as *line of no-discrimination*.

For multiple trials, the accumulation of points *above* the diagonal indicates high predicting ability

and *vice versa*. Therefore, the *area* under ROC curve is a commonly used metric for measuring predictive performance of a binary classification algorithm.

B.2 Application to Seizure Prediction

This section applies the theory of Receiver Operating Characteristic (ROC) to seizure prediction. How do we express the *true positive* TP, *false positive* FP, *true negative* TN, and *false negative* FN in terms of EEG parameters relevant for seizure prediction? Consider the drawing in Figure B.3

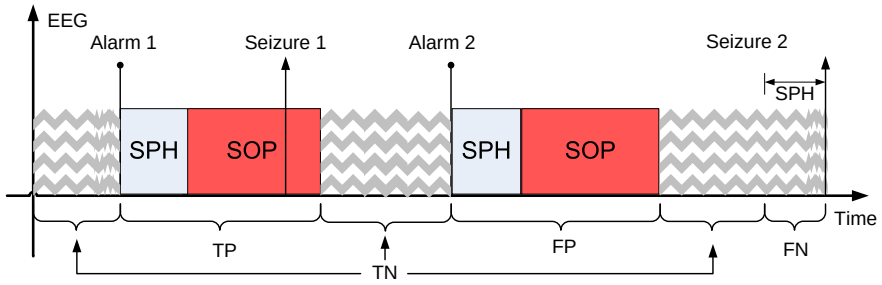

Figure B.3: Seizure Prediction Metrics

In Figure B.3, SOP refers to the Seizure Occurrence Period and stands for the period of time within which a seizure is expected to occur. SPH is an acronym for Seizure Prediction Horizon and measures how far ahead a given algorithm can predict a rising seizure. [2]

Therefore, a *true positive* TP is incremented whenever a seizure occurs within SOP. A *false positive* FP is increased when a seizure does *not* occur within SOP. A *false negative* FN is incremented when a seizure does develop but is not preceded by an alarm within SPH. Note, that this is a stricter definition than requiring the seizure to be preceded by an alarm within $SPH + SOP$ time

[2] See Section 2.3.2 for detailed discussion on SPH and SOP

period. A less trivial question is how to define a *true negative* TN, the case when a seizure does not occur and we do not predict it?

In theory, every single time window, which is outside the SPH and does not produce an alarm, could be counted as a true negative. However, since sensitivity is defined as the number of seizures with at least one alarm emerging within SPH divided by the total number of seizures, the *true negative* TN can be defined in a *complementary* way [Figure B.3]

$$TN = \frac{TotalRecordingTime - [(TP + FP) * (SPH + SOP) + FN * SPH]}{SPH + SOP} \tag{B.7}$$

note the expression above represents the worst case TN, when every seizure arrives at the very end of SOP resulting in the maximum waiting period of $SPH + SOP$.

To construct the ROC curve, we require the knowledge of FPR. A simple definition yields

$$FPR_1 = \frac{NumberofFalsePredictions}{TotalRecordingTime} \tag{B.8}$$

This definition, however, ignores the fact that for each seizure there is a pre-ictal (SPH) period during which a prediction is *by definition* counted as true positive. Thus, an alternative definition proposed in [5] was used,

$$FPR_2 = \frac{NumberofFalsePredictions}{TotalRecordingTime - NumberofSeizures * (SPH)} \tag{B.9}$$

The revised definition is stricter, in a sense that it yields a higher false positive rate. In general, a stricter definition was always selected among the alternatives and used to analyze experimental results.